The Astrophysical Journal, 632:421–437, 2005 October 10

DYNAMICAL EVOLUTION OF NEUTRINO-COOLED ACCRETION DISKS: DETAILED MICROPHYSICS, LEPTON-DRIVEN CONVECTION, AND GLOBAL ENERGETICS

William H. Lee,[1] Enrico Ramirez-Ruiz,[2,3] and Dany Page[1]
Received 2005 March 15; accepted 2005 May 26

ABSTRACT

We present a detailed, two-dimensional numerical study of the microphysical conditions and dynamical evolution of accretion disks around black holes when neutrino emission is the main source of cooling. Such structures are likely to form after the gravitational collapse of massive rotating stellar cores or the coalescence of two compact objects in a binary (e.g., the Hulse-Taylor system). The physical composition is determined self-consistently by considering two regimes, neutrino opaque and neutrino transparent, with a detailed equation of state that takes into account neutronization, nuclear statistical equilibrium of a gas of free nucleons and α-particles, blackbody radiation, and a relativistic Fermi gas of arbitrary degeneracy. Various neutrino emission processes are considered, with $e^{\pm}$ capture onto free nucleons providing the dominant contribution to the cooling rate. We find that important temporal and spatial scales, related to the optically thin/optically thick transition, are present in the disk and manifest themselves clearly in the energy output in neutrinos. This transition produces an inversion of the lepton gradient in the innermost regions of the flow that drives convective motions and affects the density and disk scale height radial profiles. The electron fraction remains low in the region close to the black hole and, if preserved in an outflow, could give rise to heavy-element nucleosynthesis. Our specific initial conditions arise from the binary merger context, and so we explore the implications of our results for the production of gamma-ray bursts.

Subject headings: accretion, accretion disks — dense matter — gamma rays: bursts — hydrodynamics — neutrinos

1. INTRODUCTION

Gas accretion by a concentration of mass is an efficient way to transform gravitational binding energy into radiation (Salpeter 1964; Zel'dovich 1964) and is responsible for observable phenomena at all scales in astrophysics. The more compact the object, the greater the efficiency. In many cases, systems are observed in steady state or quasi–steady state during this process (e.g., cataclysmic variables [CVs], low-mass X-ray binaries [LMXBs], and active galactic nuclei [AGNs]). Some external agent (e.g., the interstellar medium, a companion star) provides a continuous supply of mass, energy, and angular momentum over a timescale that is much longer than the accretion time. The energy dissipated by the flow before it is accreted, and more importantly what happens to this energy, determines many of the properties of the flow itself. In most cases cooling is present through some radiative electromagnetic process, which acts as a sink, removing the dissipated energy. In the standard thin-disk theory developed by Shakura & Sunyaev (1973), it is extremely efficient, maintaining a "cool" (in the sense that $kT \ll GMm_p/r$, where M is the mass of the central object) and thin (with a scale height $H \ll r$), nearly Keplerian disk. The requirements of steady state, hydrostatic equilibrium in the vertical direction, energy and angular momentum balance, and an equation of state yield a solution for all relevant variables as a function of the disk radius, r. The key question of angular momentum transport was addressed by Shakura & Sunyaev (1973) with their famous α prescription, which allows a parameterization of the viscous stresses and energy dissipation rates. Magnetic fields could be at the physical origin of this effect, through the magnetorotational instability (MRI; Balbus & Hawley 1991; Hawley & Balbus 1991). In the case of inefficient cooling, a solution was found in the 1970s for so-called slim disks (Shapiro et al. 1976), and later for a class that became known as ADAFs (advection-dominated accretion flows; Ichimaru 1977; Narayan & Yi 1994, 1995; Abramowicz et al. 1995). In this case, the cooling is negligible, either because the optical depth is large or because the density is so low that the radiative efficiency is extremely small. The dissipated energy is advected with the flow and may be absorbed by the central object. Such flows are geometrically thick, with scale heights $H \simeq r$. What little radiation does emerge from them arises, as in the thin disks, through various electromagnetic processes.

In either of the above scenarios, accretion (and the accompanying radiation) is usually thought to be limited by the Eddington rate, a self-regulatory balance imposed by Newtonian gravity and radiation pressure. The standard argument gives a maximum luminosity $L_{\rm Edd} = 1.3 \times 10^{38}(M/M_{\odot})$ ergs s^{-1}. Although this may not be strictly the case in reality, as in the current argument concerning the nature of ultraluminous X-ray sources (ULXs) observationally (Rappaport et al. 2005; King & Dehnen 2005) and also quite general theoretical considerations (Abramowicz 2004), it does exhibit the qualitative nature of the effect of radiation pressure on accreting plasma, in the limit of large optical depth.

The problem is circumvented (or at least deferred by nearly 16 orders of magnitude in luminosity) if the main cooling agent is emission of neutrinos, instead of photons. This regime requires correspondingly large accretion rates, of the order of 1 $M_{\odot}$ s^{-1}, and is termed hypercritical accretion (Chevalier 1989). It is important, for example, in the context of postsupernova fallback accretion onto a proto–neutron star. In such a situation, the densities and temperatures are so large ($\rho \simeq 10^{12}$ g cm^{-3}, $T \simeq 10^{11}$ K) that photons are completely trapped, and energetic neutrinos are

[1] Instituto de Astronomía, Universidad Nacional Autónoma de México, Apartado Postal 70-264, Cd. Universitaria, Mexico DF 04510, Mexico.
[2] School of Natural Sciences, Institute for Advanced Study, Einstein Drive, Princeton, NJ 08540.
[3] Chandra Fellow.

emitted in large amounts, cooling the gas and allowing accretion to proceed. The reader may wish to consult the very clear introduction in this context given by Houck & Chevalier (1991). When the stellar envelope experiences fallback onto the central object, the system may be considered to be nearly in a steady state because of the timescales involved. There are other, more violent situations, relevant to the study of gamma-ray bursts (GRBs) in which the assumption of steady state is not justified because of a time-varying mass and energy supply, and which therefore require a dynamical analysis for their proper description.

In general, whether the system cools via electromagnetic radiation or neutrinos, analytic steady state solutions are found by assuming that the cooling is either efficient (thin disk) or inefficient (thick disk). Over the last several years, many groups have considered these cases in the neutrino-cooled regime (Popham et al. 1999; Narayan et al. 2001; Kohri & Mineshige 2002; DiMatteo et al. 2002; Yokosawa et al. 2004) and established the general features of the solutions. The real solution may be very different, in particular (and in what concerns us for the following) because of the previous history of the gas that constituted the accretion disk and how the disk formed. It turns out that this may be quite important in the case of GRBs. Numerical analysis of the evolution of the disk with no assumptions concerning the steady state has been carried out by Setiawan et al. (2004). They have reported a three-dimensional calculation with detailed microphysics. Unfortunately, computational limitations do not allow one to continue such calculations for more than approximately 50 ms, whereas the typical short GRB lasts 0.2 s.

The sources of GRBs are now established (at least based on observations of X-ray, optical, and radio counterparts) to lie at cosmological distances, with redshifts $z \simeq 1$–4 (van Paradijs et al. 2000 and references therein). At such scales, the absolute energetics of each event is approximately 10^{52} ergs, assuming isotropic emission. Apparent collimation inferred from achromatic breaks in the afterglow light curve may reduce this to 10^{50} ergs, depending on the particular event (Frail et al. 2001; Panaitescu & Kumar 2001; Berger et al. 2003). Although one generally considers two classes of GRBs based on duration (shorter and longer than about 2 s; Kouveliotou et al. 1993), all afterglows to date (and the corresponding inferences) come from long bursts (although see Lazzati et al. 2001). Strong evidence in favor of an SN/GRB association (Kulkarni et al. 1998; Stanek et al. 2003; Hjorth et al. 2003) now comes from several events (albeit all relatively nearby), hinting at an underlying physical connection between the two phenomena. This is the central basis of the collapsar model (Woosley 1993; MacFadyen & Woosley 1999), in which rotation of the presupernova star allows for the creation of a massive accretion disk, fed by the infalling stellar envelope. The GRB is then powered for a fallback time, which can be long enough to account for the observed durations. In the case of short bursts there is less evidence to go on, but one possibility is that they arise from compact binary mergers, with various combinations of black holes and neutron stars in the binary (Lattimer & Schramm 1976; Paczyński 1986, 1991; Eichler et al. 1989; Narayan et al. 1992) such as in the first binary pulsar to be discovered (Hulse & Taylor 1975). The tidal disruption of one star by the other gives rise to an accretion disk that powers the GRB. A black hole is either present from the start (as a variation of the Hulse-Taylor system) or produced by the collapse of a supermassive neutron star shortly after the merger itself. In this case there is no external agent feeding the accretion disk, and thus the event is over roughly on an accretion timescale (which would be on the order of 1 s). Clearly, investigating either of these scenarios requires time-dependent, multidimensional calculations with detailed microphysics (Ruffert et al. 1996; Kluźniak & Lee 1998; Ruffert & Janka 1999; Lee 2001; Rosswog & Ramirez-Ruiz 2002; Rosswog et al. 2003, 2004). The energy released by accretion is then transformed into a relativistic outflow that produces the GRB (for reviews see Mészáros 2002; Zhang & Mészáros 2004; Piran 2004). We note that either scenario would produce a distinct gravitational wave signal, which could in principle be detected by interferometric systems such as LIGO in the future, thus establishing the nature of the progenitor system without a doubt.

The regime in which the gas lies is unlike any other commonly encountered in astrophysics. The high densities and temperatures lead to photodisintegration of the nuclei and the establishment of nuclear statistical equilibrium (NSE). Furthermore, neutronization becomes important in the innermost regions of the flow and weak interactions determine the composition, with the electron fraction falling substantially below $\frac{1}{2}$, and the gas correspondingly becoming neutron-rich. If this composition is somehow frozen and transported out of the gas and into an outflow, interesting nucleosynthesis of heavy elements could occur (Qian & Woosley 1996; Pruet et al. 2003, 2004). Realistic physics input of this kind allows us to obtain more reliable estimates of the actual energy released from the disk and potentially available to power a GRB. An added complication, which affects the composition (Beloborodov 2003), is that even if the main cooling mechanism is neutrino emission, these are not entirely free to leave the system, as scattering (mainly off free nucleons) is important enough to suppress the emission in the dense inner disk. We find that in fact the opaqueness of the material may lead to convection through the establishment of a composition gradient that does not satisfy the classical requirements for stability. To our knowledge, this is the first time that this has been addressed in this context.

In previous work we initially studied the merger process for black hole–neutron star binaries in three dimensions, paying particular attention to the structure of the accretion disks that formed as a result of the tidal disruption (Lee 2001). Follow-up work used the results of these simulations, mapped to two dimensions in azimuthal symmetry, as initial conditions with simple (ideal gas) input physics and no realistic cooling included (Lee & Ramirez-Ruiz 2002). A first approximation at a realistic equation of state and the effects of neutrino opacities was reported more recently (Lee et al. 2004).

In this paper we improve on our earlier results in three important ways that make them more realistic and particularly relevant to the study of GRBs. First, we use a much more detailed equation of state, appropriate for the actual physical conditions found in postmerger accretion disks. This includes a relativistic electron gas of arbitrary degeneracy, radiation pressure, and an ideal gas of free nucleons and α-particles. The composition is determined self-consistently by considering weak interactions in two different regimes: neutrino opaque and neutrino transparent. Second, we include neutrino emission as the main source of cooling, by considering the relevant reaction rates (electron and positron capture onto free nucleons, bremsstrahlung, pair annihilation, and plasmon decays), taken from tables and fitting formulae valid over wide ranges of temperature and density whenever possible. Third, we compute an approximate optical depth for the fluid to neutrinos, using scattering off free nucleons and α-particles as a source of opacity. The emission rates and pressure due to neutrinos are then suppressed and enhanced, respectively, by an appropriate factor.

We begin this paper by a presentation of the physical conditions likely to occur in postmerger accretion disks in § 2,

immediately following the coalescence of the two compact objects. Our results follow in § 3, and a discussion of these, as well as the implications they have for GRBs, is presented in § 4.

2. POSTMERGER ACCRETION DISKS

The accurate study of the dynamical evolution of the accretion disks requires knowledge of the physical conditions within them and the use of an appropriate equation of state. Below we give a general overview of the physical conditions in the disk, followed by a detailed presentation of the equation of state and the effects of neutrinos.

2.1. *Physical Conditions*

The accretion structures that are formed as a result of the merger of two neutron stars or the tidal disruption of a neutron star by the black hole become azimuthally symmetric fairly quickly, within a few tens of milliseconds (Ruffert et al. 1996; Lee 2001). These disks typically contain a few tenths of a solar mass and are small, with the bulk of the mass being contained within 200 km of the black hole (which harbors about 3–5 $M_\odot$). The disks are dense (10^9 g cm$^{-3} \le \rho \le 10^{12}$ g cm^{-3}), with high internal energies (10^{10} K $\le T \le 10^{11}$ K; see, e.g., Ruffert & Janka 1999; Rosswog et al. 1999; Lee & Ramirez-Ruiz 2002). In fact, the temperature is high enough that nuclei become photodisintegrated and there is a mixture of α-particles, free neutrons and protons, electrons, and positrons. The timescale for β equilibrium is given by $t_\beta \approx (\sigma_{Ne} n_N c)^{-1}$, where σ_{Ne} is the cross section for $e^\pm$ capture onto free nucleons and n_N is the number density of free nucleons (see, e.g., Shapiro & Teukolsky 1983). Under these conditions, $t_\beta \approx 2 \times 10^{-4}$ s, which is much shorter than the accretion timescale $t_{\rm acc}$ of a fluid element, so that weak interactions determine the composition. Photons are trapped and are advected with the flow. For neutrinos the situation is more complicated, since the optical depth is of order unity. In the outer regions of the disk they escape freely, whereas for densities larger than $\approx 10^{11}$ g cm^{-3} they undergo diffusion on a timescale $t_{{\rm dif},\nu} \approx 30$ ms.

2.2. *The Equation of State and the Composition of the Fluid*

For simplicity of presentation, we first assume that all nucleons are free (no α-particles are present) and include the necessary corrections subsequently.

Under the conditions described above, the temperature is high enough for electron-positron pair creation. The number of pairs thus produced is very sensitive to the degeneracy of the electrons. In fact, the number density of pairs is suppressed exponentially with increasing degeneracy because of Fermi blocking. In previous work (Popham et al. 1999; Narayan et al. 2001; Kohri & Mineshige 2002; DiMatteo et al. 2002; Lee et al. 2004) the assumption of full degeneracy has been made for simplicity (note also that in some cases the presence of electron-positron pairs has been assumed while at the same time retaining a degeneracy pressure term, which is inconsistent). Here we take a different approach, using an exact expression for the pressure as a function of the temperature and the chemical potential, valid for arbitrary degeneracy in the limit of relativistic electrons (i.e., $\rho \ge 10^6$ g cm^{-3}), due to Blinnikov et al. (1996), namely,

$$P_e = \frac{1}{12\pi^2(\hbar c)^3}\left[\eta_e^4 + 2\pi^2\eta_e^2(kT)^2 + \frac{7}{15}\pi^4(kT)^4\right]. \quad (1)$$

The number densities of electrons and positrons are related by

$$\frac{\rho Y_e}{m_u} = n_- - n_+ = \frac{1}{3\pi^2(\hbar c)^3}\left[\eta_e^3 + \eta_e\pi^2(kT)^2\right], \quad (2)$$

where Y_e is the electron fraction. The chemical potential of species i is denoted by η_i throughout. This expression reduces to the well-known limits when the temperature is low ($kT \ll \eta_e$, which gives $P \propto \rho^{4/3}$, appropriate for a cold relativistic Fermi gas) and when it is high ($kT \gg \eta_e$, which gives $P \propto T^4$, when the pressure comes from relativistic electron-positron pairs). The full equation of state then reads

$$P = P_{\rm rad} + P_{\rm gas} + P_e + P_\nu, \quad (3)$$

where

$$P_{\rm rad} = \frac{aT^4}{3}, \quad (4)$$

$$P_{\rm gas} = \frac{\rho kT}{m_u}, \quad (5)$$

and P_ν is the pressure due to neutrinos (discussed below). Here a is the radiation constant, k is Boltzmann's constant, and $m_u = 1.667 \times 10^{-24}$ g is the atomic mass unit. Since the presence of pairs is automatically taken into account in the expression for P_e, there is no alteration to the numerical factor $\frac{1}{3}$ in the expression for $P_{\rm rad}$. For the conditions encountered in the accretion disks presented below, gas pressure dominates at the 80% level over the other terms. Regarding the photons, since the temperature is $T \approx 5$ MeV, the peak in the blackbody spectrum is at $\approx$14 MeV. On the other hand, the plasma frequency, ω_p, corresponds to $T_p \approx 0.5$ MeV. Thus, the standard expression for radiation pressure may be considered accurate and plasma effects negligible as far as the photons are concerned.

The computation of the electron fraction and the chemical potential of electrons follows from the assumption of β equilibrium between neutrons, protons, and electrons and the condition of charge neutrality. As noted by Beloborodov (2003), a distinction needs to be made to determine the equilibrium composition depending on the optical depth of the material (the determination of the opacities is presented in § 2.4). If it is transparent to its own neutrino emission, we fix equilibrium by equating the capture rates of electrons and positrons onto protons and neutrons, respectively. For mild degeneracy, as is the case here, this leads to the following expression for the electron fraction as a function of the temperature and the electron chemical potential (Beloborodov 2003):

$$Y_e = \frac{1}{2} + 0.487\left(\frac{Q/2 - \eta_e}{kT}\right), \quad (6)$$

where $Q = (m_n - m_p)c^2 \simeq 1.29$ MeV. If, however, the material is opaque and the neutrinos are allowed to diffuse out on a timescale shorter than the accretion timescale, then we may write

$$\eta_e + \eta_p = \eta_n, \quad (7)$$

for the equilibrium composition.[4] Since the nucleons are not degenerate, we may use Maxwell-Boltzmann statistics to describe their distribution function and obtain

$$\frac{n_p}{n_n} = \exp\left(\frac{Q-\eta_e}{kT}\right) \tag{8}$$

for the ratio of proton to neutron number densities. Further, with $Y_e = n_p/(n_p+n_n)$ we arrive at

$$\frac{1-Y_e}{Y_e} = \exp\left(\frac{\eta_e - Q}{kT}\right). \tag{9}$$

We now have the three equations (2), (3), and (6) or (9) for the three functions T, Y_e, and η_e and so the system is closed. To allow for a transition from the optically thin to optically thick regime, in fact we solve these in a combined form, weighted by factors $f(\tau_\nu) = \exp(-\tau_\nu)$ or $g(\tau_\nu) = 1 - \exp(-\tau_\nu)$. As a practical matter, the internal energy per unit mass, u, is used instead of the pressure to solve equation (3), since its variation in time is what is determined in the code, using the first law of thermodynamics. We finally include the effects of incomplete photodisintegration of α-particles by using nuclear statistical equilibrium for the three species (n, p, α) to fix the mass fraction of free nucleons as (Qian & Woosley 1996)

$$X_{\rm nuc} = 22.4\left(\frac{T}{10^{10}\ {\rm K}}\right)^{9/8}\left(\frac{\rho}{10^{10}\ {\rm g\ cm^{-3}}}\right)^{-3/4} \times \exp\left(-8.2\frac{10^{10}\ {\rm K}}{T}\right). \tag{10}$$

Whenever this expression results in $X_{\rm nuc} > 1$, we set $X_{\rm nuc} = 1$. The corresponding alterations in the previous derivation are simple and lead to the full set of equations that we write for each gas element and at each time. Note that these do not allow for an explicit solution, so an iterative scheme is used in each instance. The internal energy per unit mass is

$$u = 3\frac{P_e + P_{\rm rad} + P_\nu}{\rho} + \frac{1+3X_{\rm nuc}}{4}\frac{3kT}{2m_u}, \tag{11}$$

β equilibrium gives

$$Y_e = \frac{1-X_{\rm nuc}}{2} + X_{\rm nuc}\left\{\left[\frac{1}{2} + 0.487\left(\frac{Q/2-\eta_e}{kT}\right)\right]f(\tau_\nu) + \left[1 + \exp\left(\frac{\eta_e - Q}{kT}\right)\right]g(\tau_\nu)\right\}, \tag{12}$$

and charge neutrality implies

$$\frac{\rho Y_e}{m_u} = \frac{1}{3\pi^2(\hbar c)^3}\left[\eta_e^3 + \eta_e\pi^2(kT)^2\right], \tag{13}$$

as given by equation (2). The modifications to the equation for β equilibrium simply reflect the fact that if the fluid is composed primarily of α-particles, there will be one neutron per proton, and hence $Y_e \to \frac{1}{2}$.

[4] This expression neglects the neutrino chemical potential, η_ν, and is strictly valid only when there are equal numbers of neutrinos and antineutrinos. Otherwise the electron pressure, bulk viscosity, and Joule-like heating due to the induced lepton current will be affected (Burrows et al. 1981; Socrates et al. 2004). We neglect all these corrections in the present treatment.

2.3. *Neutrino Emission and Photodisintegration Losses*

Several processes contribute to the emission of neutrinos. First, we take into account electron and positron capture onto free nucleons using the tables of Langanke & Martínez-Pinedo (2001). This is an improvement over calculations done previously (Popham et al. 1999; Narayan et al. 2001; Kohri & Mineshige 2002; DiMatteo et al. 2002; Lee et al. 2004), where assumptions concerning the degeneracy were made. The rates are thus accurate over the entire disk, whether the degeneracy is significant or not. The tables cover the ranges $1 \le \log[\rho Y_e({\rm g\ cm^{-3}})] \le 11$ and $7 \le \log T({\rm K}) \le 11$. A bilinear interpolation in the $\log \rho Y_e - \log T$ plane is performed using the table to obtain the cooling rate for a given mass element. The result is then multiplied by the mass fraction of free nucleons, $X_{\rm nuc}$, since we are not considering capture of electrons and protons by α-particles. Second, the annihilation of electron-positron pairs is a source of thermal neutrinos, and the corresponding cooling rate is computed using the fitting functions of Itoh et al. (1996). These cover the range $9 \le \log[\rho({\rm g\ cm^{-3}})] \le 12$ in density and $10 \le \log T({\rm K}) \le 11$ in temperature. Finally, nucleon-nucleon bremsstrahlung, $\dot{q}_{\rm ff}$, and plasmon decay, $\dot{q}_{\rm plasmon}$, are considered, with rates given by

$$\dot{q}_{\rm ff} = 1.5\times10^{33}T_{11}^{5.5}\rho_{13}^2\ {\rm ergs\ s^{-1}\ cm^{-3}} \tag{14}$$

(Hannestad & Raffelt 1998) and

$$\dot{q}_{\rm plasmon} = 1.5\times10^{32}T_{11}^9\gamma_p^6\exp(-\gamma_p)(1+\gamma_p) \times\left(2+\frac{\gamma_p^2}{1+\gamma_p}\right)\ {\rm ergs\ s^{-1}\ cm^{-3}}, \tag{15}$$

where $\gamma_p = 5.5\times10^{-2}\{[\pi^2 + 3(\eta_e/kT)^2]/3\}^{1/2}$ (Ruffert et al. 1996). For the conditions encountered in the disk, capture by nucleons completely dominates all other processes and is the main source of cooling. Finally, the creation and disintegration of α-particles lead to a cooling term in the energy equation given by

$$\dot{q}_{\rm phot} = 6.8\times10^{18}\frac{dX_{\rm nuc}}{dt}\ {\rm ergs\ s^{-1}\ cm^{-3}}. \tag{16}$$

2.4. *Neutrino Opacities*

The material in the disk is dense enough that photons are completely trapped and advected with the flow. For neutrinos, however, the situation is more complicated, since the outer regions are transparent to them, while the inner portions are opaque.

The main source of opacity is scattering off free nucleons and α-particles, with cross sections given by (Tubbs & Schramm 1975; Shapiro & Teukolsky 1983)

$$\sigma_N = \frac{1}{4}\sigma_0\left(\frac{E_\nu}{m_ec^2}\right)^2 \tag{17}$$

and

$$\sigma_\alpha = \sigma_0\left(\frac{E_\nu}{m_ec^2}\right)^2\left[\left(4\sin^2\theta_{\rm W}\right)\right]^2, \tag{18}$$

where $\sigma_0 = 1.76\times10^{-44}$ cm^2 and $\theta_{\rm W}$ is the Weinberg angle. Since capture processes dominate the neutrino luminosity, we assume that the mean energy of the neutrinos is roughly equal to

the Fermi energy of the partially degenerate electrons $E_\nu \approx \frac{5}{6}\eta_e = 43(Y_e\rho_{12})^{1/3}$ MeV, where $\rho_{12} = \rho/10^{12}$ g cm^{-3}. So the mean free path is $l_\nu = 1/(n_N\sigma_N + n_\alpha\sigma_\alpha)$, n_N and n_α being the number densities of free nucleons and α-particles, respectively. To compute an optical depth, we take $\tau_\nu = H/l_\nu$, with H a typical scale height of the disk. Inspection of the disk shape (through the density contours in the inner regions) and an estimation of the scale height with $H \simeq \rho/\nabla\rho$ suggest that $H \simeq \kappa r$, with κ a constant of order unity, so that our final, simplified expression for the optical depth reads $\tau_\nu = \kappa r/l_\nu$. With the above expressions for the cross section as a function of density and electron fraction and defining $r_7 = r/10^7$ cm, we arrive at

$$\tau_\nu = 186.5\kappa\rho_{12}^{5/3}Y_e^{2/3}r_7\left[X_{\rm nuc} + \frac{3.31(1 - X_{\rm nuc})}{4}\right]. \quad (19)$$

The term that depends on $X_{\rm nuc}$ reflects the two-species composition we have assumed. Its influence is limited, since when $X_{\rm nuc}$ varies from 0 to 1, the optical depth is altered by a factor of 1.2, all other values being equal. In practice, and for the compositions found in the disks, this expression corresponds to having an optical depth of unity at approximately 10^{11} g cm^{-3}, which can be thought of as a neutrino surface, where the last scattering occurs and neutrinos leave the system. Accordingly, we modify the expressions for the neutrino emission rates, suppressing it in the opaque regions and enhancing the pressure through

$$\left(\frac{du}{dt}\right)_\nu = \left(\frac{du}{dt}\right)_0 \exp(-\tau_\nu) \quad (20)$$

and

$$P_\nu = \tfrac{7}{8}aT^4[1 - \exp(-\tau_\nu)], \quad (21)$$

where $(du/dt)_0 = \sum \dot{q}_i/\rho$ is the unmodified energy loss rate (in ergs g^{-1} s^{-1}) calculated from the rates given in § 2.3.

The total neutrino luminosity (in ergs s^{-1}) is then computed according to

$$L_\nu = \int \rho^{-1}\left(\dot{q}_{\rm ff} + \dot{q}_{\rm plasmon} + \dot{q}_{\rm pair} + \dot{q}_{\rm cap}\right)\exp(-\tau_\nu)\, dm. \quad (22)$$

2.5. *Numerical Method and Initial Conditions*

For the actual hydrodynamical evolution calculations, we use the same code as in previous work (Lee & Ramirez-Ruiz 2002) and refer the reader to that paper for the details. This is a two-dimensional [cylindrical coordinates (r, z) in azimuthal symmetry] smoothed particle hydrodynamics (SPH) code (Monaghan 1992), modified from our own three-dimensional version used for compact binary mergers (Lee 2001). The accretion disk sits in the potential well of a black hole of mass $M_{\rm BH}$, which produces a Newtonian potential $\Phi = -GM_{\rm BH}/r$. Accretion is modeled by an absorbing boundary at the Schwarzschild radius $r_{\rm Sch} = 2GM_{\rm BH}/c^2$, and the mass of the hole is updated continuously. The transport of angular momentum is modeled with an α viscosity prescription, including *all* components of the viscous stress tensor (not only $t_{r\phi}$). The self-gravity of the disk is neglected.

The main modifications from the previous version are in the implementation of a new equation of state (§ 2.2), neutrino emission (§ 2.3), and the treatment of neutrino optical depths (§ 2.4).

TABLE 1
Initial Conditions for the Accretion Disks

Run[a]	α	$M_{\rm BH}$[b] ($M_\odot$)	$M_{\rm disk}$[b] ($M_\odot$)	N[c]
aIM	0.0	3.85	0.308	19772
a1M	0.1	3.85	0.308	19772
a2M	0.01	3.85	0.308	19772
a3M	0.001	3.85	0.308	19772
a1m	0.1	3.85	0.062	19772
a2m	0.01	3.85	0.062	19772
a3m	0.001	3.85	0.062	19772

[a] In the run label, the number refers to the value of α (with "I" standing for inviscid, with $\alpha = 0$) and the letter to high (M) or low (m) disk mass.
[b] Values at the start of the two-dimensional calculation of the accretion disk evolution.
[c] Number of SPH particles at the start of the two-dimensional calculation.

As done previously (Lee & Ramirez-Ruiz 2002; Lee et al. 2004), the initial conditions are taken from the final configuration of three-dimensional calculations of black hole–neutron star mergers, after the accretion disk that forms through tidal disruption of the neutron star has become fairly symmetric with respect to the azimuthal coordinate. We show in Table 1 the parameters used in each of the dynamical runs included in this paper.

3. RESULTS

As the dynamical evolution calculations begin, the disks experience an initial transient, which is essentially numerical in origin and is due to the fact that the configuration is not in strict hydrostatic equilibrium (recall that it is obtained from azimuthally averaging the results of three-dimensional calculations). This transient and its effects are negligible, and it is essentially over in a hydrodynamical timescale (≈2 ms). After that, the disk proceeds to evolve on a much longer timescale, determined by accretion onto the central black hole. We first present the details of the spatial structure of the disk due to fundamental physical effects and then proceed to show the temporal evolution and associated transitions.

3.1. *Disk Structure*

The fundamental variable affecting the instantaneous spatial structure of the disk is the optical depth to neutrinos, τ_ν, since it determines whether the fluid cools efficiently or not. All quantities show a radical change in behavior as the threshold $\tau_\nu = 1$ is passed. Figure 1 shows color-coded contours in a meridional slice of the thermodynamical variables, while Figure 2 displays the run of density and entropy per baryon along the equator, $z = 0$, where the density and temperature are highest (we refer here mainly to run a2M, unless noted otherwise). The density increases as one approaches the black hole, varying as $\rho \propto r^{-5}$ in the outer regions, where $\tau_\nu \ll 1$. The critical density for opaqueness is reached at $r_* \simeq 10^7$ cm, and for $r < r_*$, $\rho \propto r^{-1}$. Since the energy that would otherwise be lost via neutrino emission remains in the disk if the cooling is suppressed by scattering, the density does not rise as fast. In fact, one can note this change also by inspecting the scale height $H \simeq P/\nabla P$, which scales as $H/r \propto r$ for $r > r_*$ and $H/r \propto$ const for $r < r_*$ (and thus in terms of surface density the change is from $\Sigma \propto r^{-4}$ to $\Sigma \propto$ const at r_*). The opaque region of the disk remains inflated to a certain extent, trapping the internal energy it holds and releasing it only on a diffusion timescale. At densities $\rho \simeq 10^{12}$ g cm^{-3} the optical

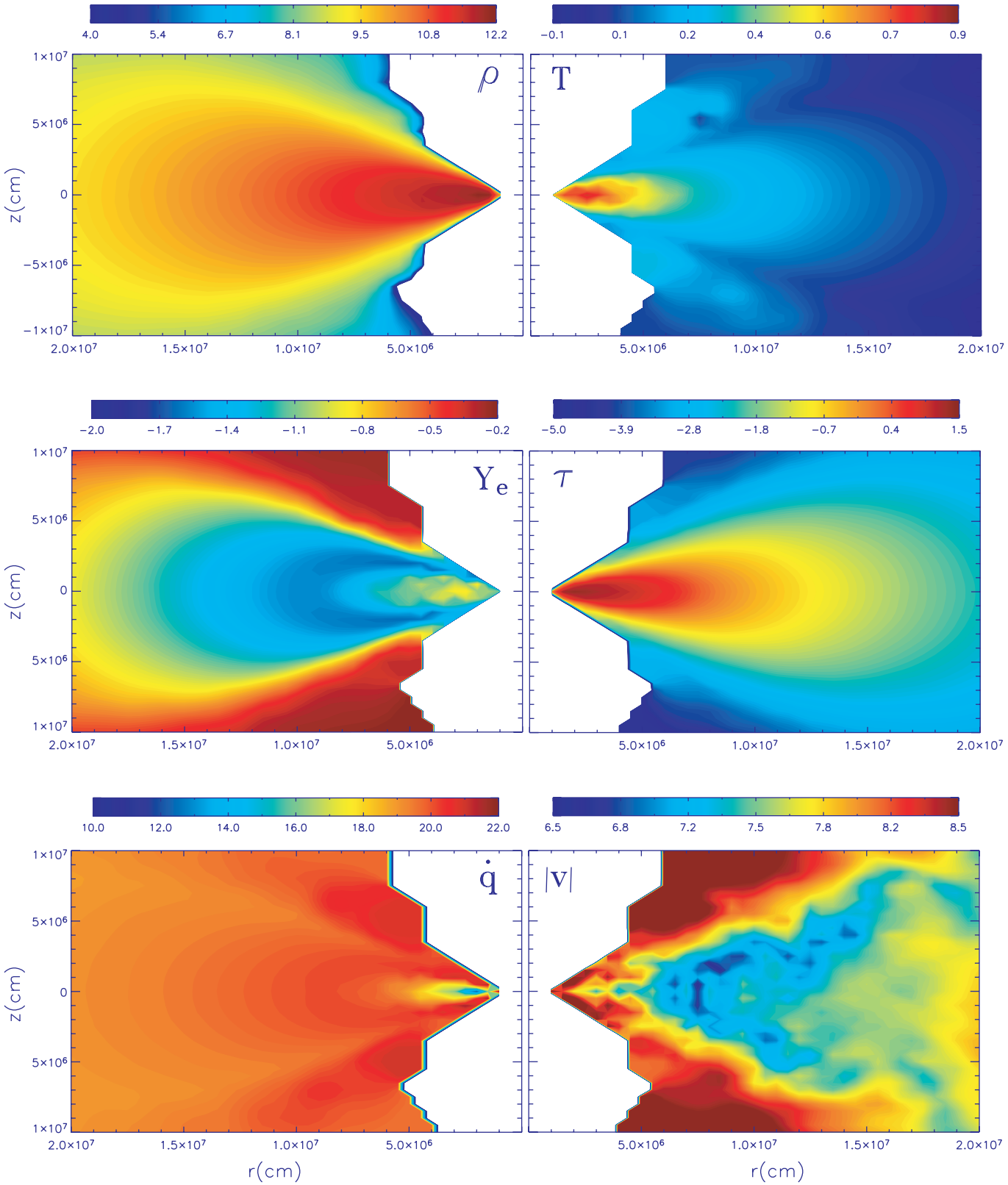

FIG. 1.—Color-coded logarithmic contours of density (g cm^{-3}), temperature (MeV), electron fraction, optical depth, cooling (ergs g^{-1} s^{-1}), and magnitude of velocity (cm s^{-1}) for run a2M at $t = 100$ ms. The qualitative change in composition is clearly seen in the contours of Y_e when the material becomes optically thick (note also the exponential suppression of cooling in the contours of $\dot{q}$ in this regime). See text for details.

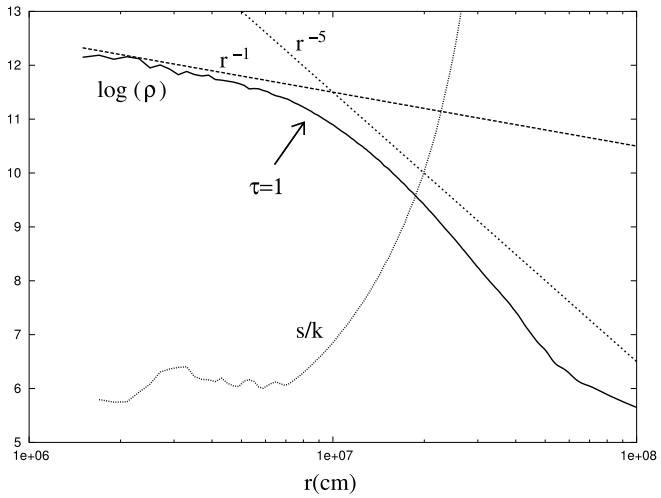

FIG. 2.—Density and entropy per baryon, s/k, along the equatorial plane, $z = 0$, for run a2M at $t = 100$ ms, as in Fig. 1. Note the logarithmic scale in density and the sharp transition and change in behavior from the optically thin to optically thick regimes. Reference power laws for the density profile are indicated. In the optically thick region, the entropy per baryon is practically constant.

depth can reach $\tau_\nu \simeq 100$, and thus the suppression of cooling is dramatic, as can be seen in Figure 1, where the contours of τ_ν and $\dot{q}$ are shown. The flattening of the entropy profile is related to the change in composition in the optically thick region and the occurrence of convection (see § 3.2).

As the density rises in the inner regions of the disk, the electron fraction Y_e initially drops as neutronization becomes more important, with the equilibrium composition being determined by the equality of electron and positron captures onto free neutrons and protons (see eq. [6] and the discussion preceding it). The lowest value is reached at $r \simeq r_*$, where $Y_e \simeq 0.03$. Thereafter it rises again, reaching $Y_e \simeq 0.1$ close to the horizon. Thus, flows that are optically thin everywhere will reach a higher degree of neutronization close to the black hole than those that experience a transition to the opaque regime. The numerical values for the electron fraction at the transition radius and at the inner boundary are largely insensitive to α, as long as the transition does occur.

The baryons in the disk are essentially in the form of free neutrons and protons, except at very large radii and low densities ($r > 5 \times 10^7$ cm and $\rho < 5 \times 10^6$ g cm^{-3}) where α-particles form. Figure 3 shows the region in the density-temperature plane where the fluid lies, for runs a2M and a1M at two different times (and color coded according to the electron fraction). Most of the

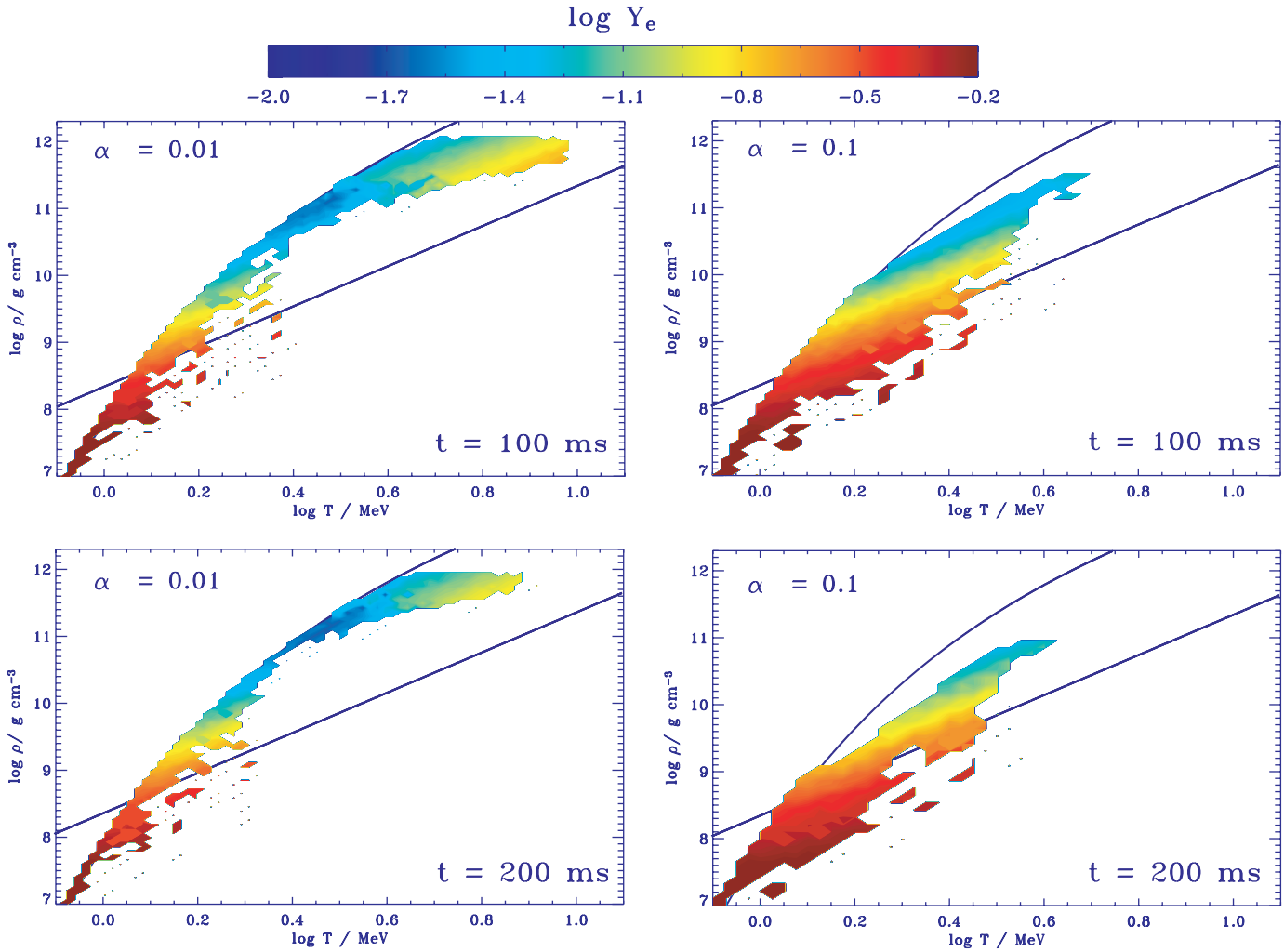

FIG. 3.—Color-coded electron fraction in the ρ-T plane for runs a2M (*left*) and a1M (*right*) at $t = 100$ (*top*) and 200 ms (*bottom*). The solid curving line marks the transition in composition from free nucleons (at high temperatures and low densities) to α-particles (at low temperatures and high densities). The solid straight line marks the degeneracy threshold, given by $kT = 7.7\rho_{11}^{1/3}$ MeV.

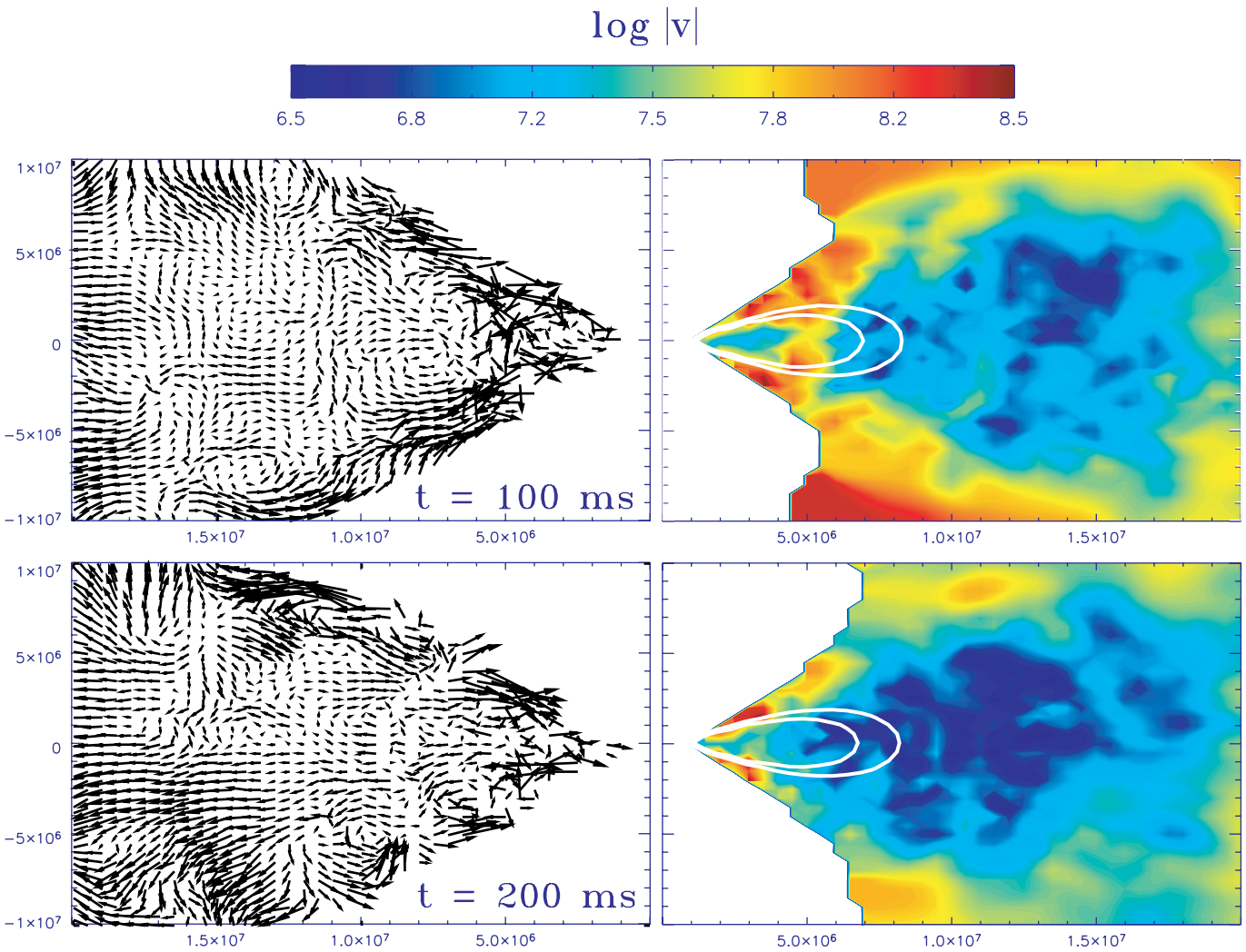

FIG. 4.—Velocity field (*left*) and color-coded velocity contours (*right*) for run a2M at $t = 100$ (*top*) and 200 ms (*bottom*), showing clearly the small-scale circulations present in the disk (the units are cm s^{-1}). The solid white contours correspond to optical depths $\tau = 3/2$ and 6.

gas lies close to the line determining the formation of helium nuclei (see eq. [10]) but does not cross over to lower temperatures. The reason for this is that the energy that would be released by the creation of one helium nucleus (28.3 MeV) would not leave the disk (recall that we consider neutrino emission as the only source of cooling) and thus immediately lead to the photodisintegration of another α-particle. An equilibrium is thus maintained in which the gas is close to helium synthesis, but this does not occur. In the opaque regime, the gas moves substantially farther from the transition line to helium, since it cannot cool efficiently and, as mentioned before, the density does not rise as quickly. Figure 3 also shows clearly why one must make use of an equation of state that takes into account properly the effects of arbitrary degeneracy of the electrons and positrons. The solid straight line marks the degeneracy temperature as a function of density, given by $kT = 7.7\rho_{11}^{1/3}$ MeV. The disk straddles this line, with a degeneracy parameter $\eta_e/kT \simeq 2$–4 in the inner regions and $\eta_e/kT \approx 1$ at lower densities. Thus, making the approximation that the electrons in the flow are fully degenerate is not accurate.

Modeling the accretion flow in two dimensions (r, z), without the assumption of equatorial symmetry, allows one to solve clearly for the vertical motions in the disk, something that is not possible when considering vertically integrated flows. It was pointed out by Urpin (1984) that a standard α viscosity could lead to meridional flows in which v_r changed sign as a function of height above the midplane, leading to inflows as well as outflows. Kita (1995), Kluźniak & Kita (2000), and Regev & Gitelman (2002) later considered a similar situation and found that for a range of values in α, the gas flowed inward along the surface of the disk and outward in the equatorial regions. In previous work (Lee & Ramirez-Ruiz 2002), we found this solution in disk flow, with large-scale circulations exhibiting inflows and outflows for high viscosities ($\alpha \simeq 0.1$) and small-scale eddies at lower values ($\alpha \leq 0.01$). How vertical motions affect the stability of accretion disks and may lead to the transport of angular momentum is a question that has become of relevance in this context (Arlt & Urpin 2004). Here we show in Figure 4 the velocity field and magnitude of meridional velocity for run a2M. The small-scale eddies are clearly visible, with their strength usually diminishing as the disk is drained of matter and the density drops. The effect of a different value of α can be seen in the top row of Figure 5, where the comparison between $\alpha = 0.1$ and 0.01 is made. The large, coherent lines of flow aimed directly at the origin for $\alpha = 0.1$ correspond to inflow, while the lighter shades along the equator at larger radii

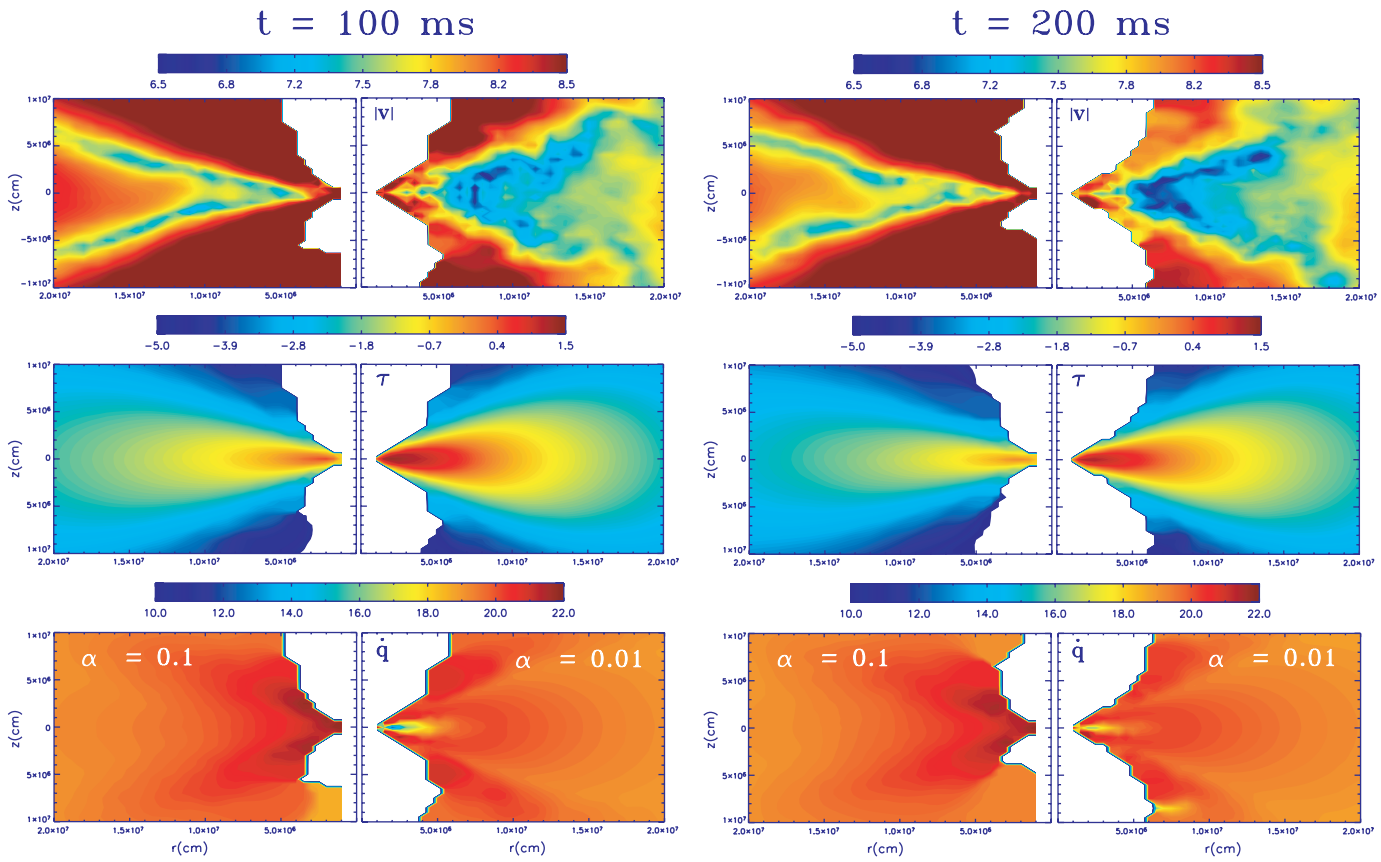

FIG. 5.—Color-coded logarithmic contours of magnitude of velocity (*top*; in cm s^{-1}), optical depth (*middle*), and cooling (*bottom*; in ergs g^{-1} s^{-1}) for runs a1M (*left half of each panel*) and a2M (*right half of each panel*), at $t = 100$ (*left column*) and 200 ms (*right column*). Note the strong thinning of the disk in the case with high viscosity, $\alpha = 0.1$, visible in the changing contours of optical depth.

show outflowing gas. Figure 6 again shows the location of the fluid in the density-temperature plane for runs a2M and a1M (as in Fig. 3), but color coded according to the optical depth to neutrinos.

The instantaneous structure of the disk concerning the density, temperature, and composition profiles is largely independent of the viscosity, as long as there is enough mass to produce the optically thin/optically thick transition. Even in the optically thin regime, the structure cannot be determined analytically following the standard arguments applied to thin, cool disks of the Shakura-Sunyaev type. The reason for this is the following: a central assumption in the standard solution is that the disk is cool, i.e., $kT/m_p \ll GM_{\rm BH}/r$. This comes from the requirement that all the energy dissipated by viscosity, $\dot{q}_\alpha$, be radiated away efficiently and produce the observed flux, F. In our case, the disk is most certainly not cool, as it originates from the tidal disruption of a neutron star by a black hole (or possibly the coalescence of two neutron stars and subsequent collapse of the central mass to a black hole). The gas that constitutes the disk is dynamically hot because it was in hydrostatic equilibrium in a self-gravitating configuration, where $U \simeq -W$, and has not been able to release this internal energy (the merger process itself may lead to additional heating). A further deviation from the standard solution is that the pressure support in the disk leads to a rotation curve that is slightly sub-Keplerian. The dissipation by viscosity is in fact smaller than the cooling rate over much of the disk, and the released luminosity comes from a combination of viscous dissipation and the store of internal energy given to the disk at its conception.

3.2. *Lepton-driven Convection*

The classical requirement for convective instability in the presence of entropy and composition gradients, as well as rotation, is the Solberg-Hoiland criterion (Tassoul 1978):

$$N^2 + \omega_r^2 < 0, \tag{23}$$

where $\omega_r^2 = 4\Omega^2 + r\,d\Omega^2/dr$ is the radial epicyclic frequency (Ω being the angular velocity) and

$$N^2 = \frac{g}{\gamma}\left[\frac{1}{P}\left(\frac{\partial P}{\partial s}\right)_{Y_e}\frac{ds}{dr} + \frac{1}{P}\left(\frac{\partial P}{\partial Y_e}\right)_s \frac{dY_e}{dr}\right] \tag{24}$$

is the Brunt-Väisäla frequency (see Lattimer & Mazurek 1981; Thompson et al. 2005). The adiabatic index $\gamma = d\ln P/d\ln\rho \approx 5/3$ in our case, since $P_{\rm gas}$ is the most important contribution to the total pressure. Thus, a region may be convectively unstable because of a composition gradient, an entropy gradient, or both. Strictly speaking, here one should consider the total lepton fraction Y_l. We do not consider the transport of neutrinos in detail, as already mentioned (see § 2.4), and do not calculate explicitly the contribution of neutrinos to this Y_l. For what follows, we thus simply take Y_e to represent the behavior of the full Y_l. The origin of convection in the lepton inversion zone can be understood as follows (Epstein 1979). Consider a fluid element in the lepton inversion zone that is displaced in the outward direction and then comes to pressure equilibrium with

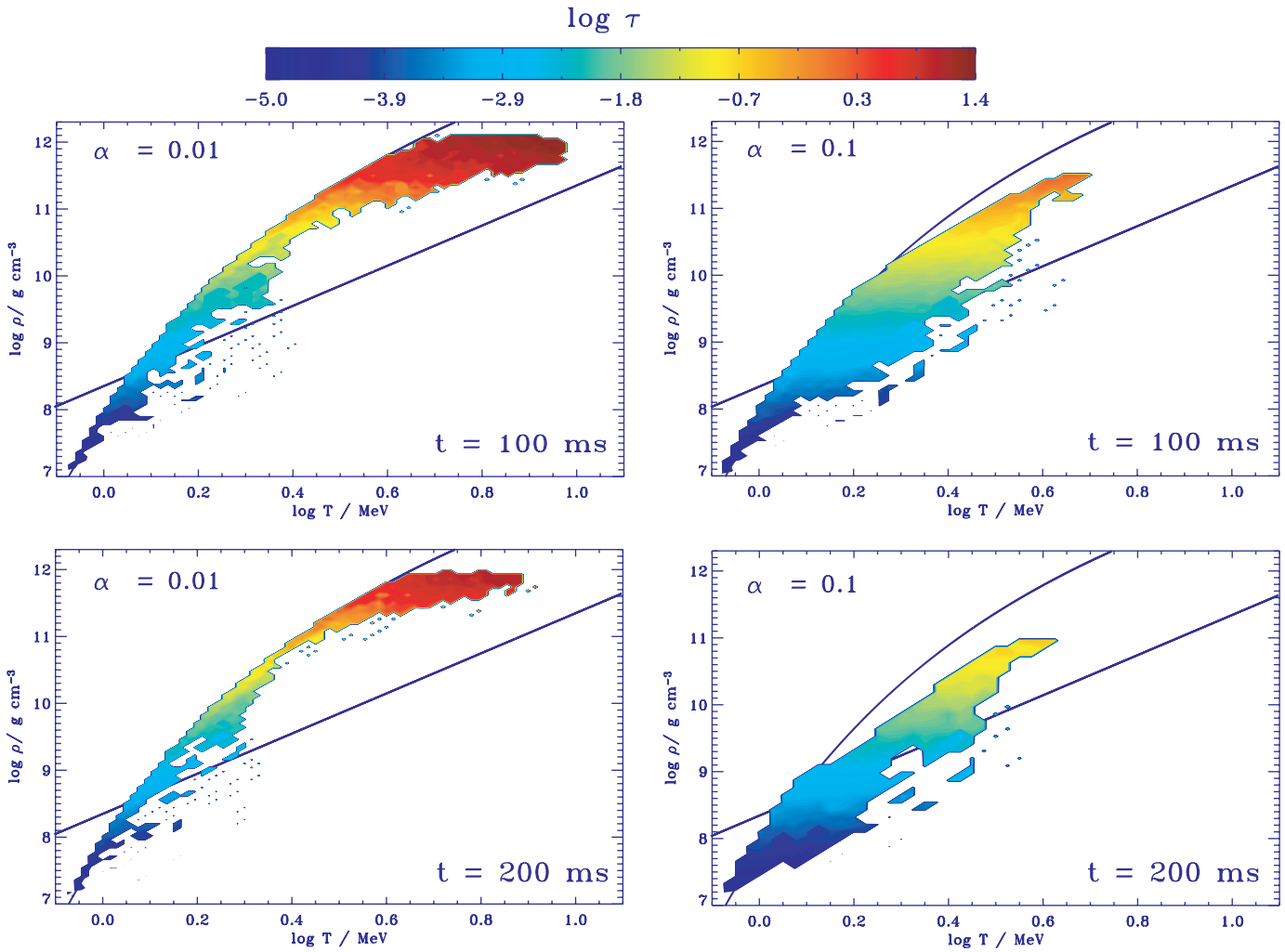

FIG. 6.—Same as Fig. 3, but color coded according to optical depth.

its surroundings. The displaced element, which is lepton-rich relative to its new surroundings, attains the ambient pressure at a lower density than the surrounding fluid because the pressure depends directly on the lepton number and thus tends to drift outward. By the same token, an inwardly displaced fluid element in the lepton inversion zone is depleted in leptons relative to its new surroundings and thus tends to sink.[5] When temperature gradients are allowed for, the displaced fluids, in general, have temperatures that differ from those of their surroundings. These variations tend to promote stability or instability depending on whether the existing temperature gradient is less than or greater than the adiabatic gradient, respectively.

In the present scenario then, the transition to the optically thick regime leads to instability because initially $ds/dr < 0$ and also $dY_e/dr < 0$ (see also Fig. 2). The entropy profile is then flattened by efficient convective mixing, and the lepton gradient inversion is due to the different way in which the composition is determined through weak interactions once the neutrinos become trapped. In a dynamical situation such as the one treated here, convection tends to erase the gradients that give rise to it. Accordingly, the sum of the corresponding terms in equation (23) tends to zero once the simulation has progressed and convection has become established in the inner disk (note that in our case the rotation curve there is sub-Keplerian, with $\Omega \propto r^{-8/5}$, so that Ω and ω_r are not equal). This is analogous to what occurs in proto–neutron stars following core collapse (Epstein 1979; Burrows & Lattimer 1986; Thompson & Duncan 1993) and has actually been confirmed in numerical simulations of such systems (Janka & Müller 1996), where the convection leads to strong mixing. For a neutrino-driven convective luminosity $L_{\rm con}$ at radius R and density ρ, the convective velocity may be estimated by standard mixing-length theory as (see, e.g., Thompson & Duncan 1993)

$$v_{\rm con} \sim 3.3 \times 10^8 \left(\frac{L_{\rm con}}{10^{52}\ {\rm ergs\ s^{-1}}}\right)^{1/3} \left(\frac{\rho}{10^{12}\ {\rm g\ cm^{-3}}}\right)^{-1/3} \times \left(\frac{R}{20\ {\rm km}}\right)^{-2/3} {\rm cm\ s^{-1}}, \quad (25)$$

where we have used the fact that gas pressure dominates in the fluid. The assumption of spherical symmetry implicit in this expression is not strictly met in our case, but it may provide us nevertheless with a useful guide. The overturn time of a convective cell is then given by $t_{\rm con} \sim l_p/v_{\rm con} \sim 10$ ms, where $l_p \sim 20$ km is the mixing length, usually set to a pressure scale height. In our calculations, we see that the magnitude of the meridional velocity $|v| = (v_r^2 + v_z^2)^{1/2}$ decreases as r decreases,

[5] This is similar to the thermosolutal convection that would occur in a normal star if there were an inwardly decreasing molecular weight gradient or composition inversion (Spiegel 1972).

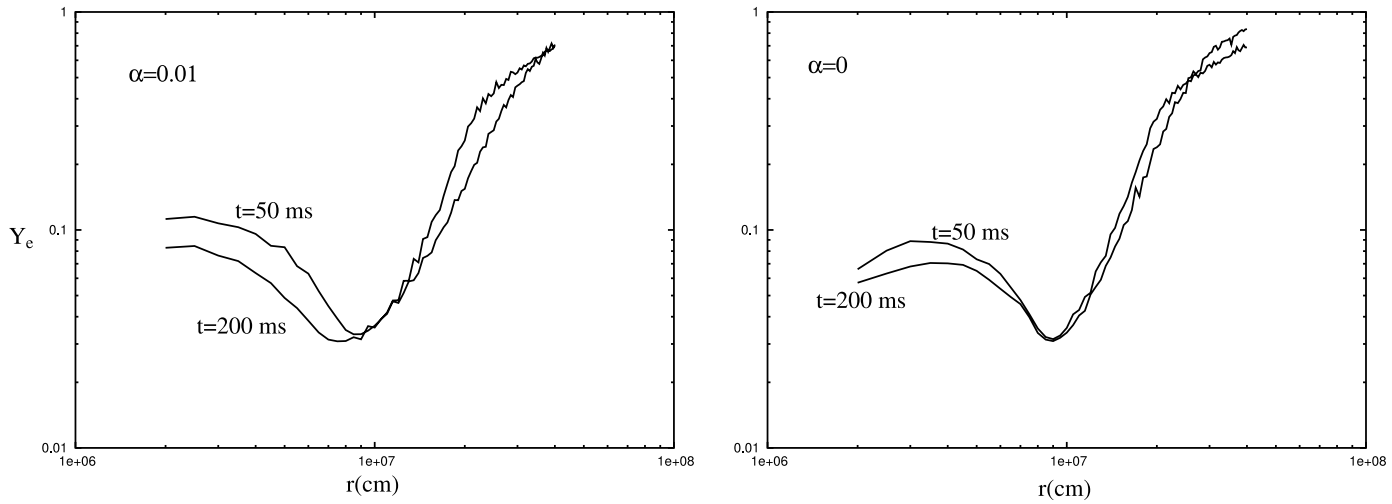

FIG. 7.—Averaged profiles of the electron fraction $Y_e(r)$ for run a2M (*left*) at $t = 50$ and 200 ms and run aIM (*right*) at $t = 50$ and 200 ms. In the inviscid calculation convection is able to suppress the composition gradient in a few characteristic turnover times, while the continuous radial motions induced by a finite value of α prevent this from happening in the run with viscosity.

then rises again as the opaque region is reached, reaching $|v| \simeq 10^8$ cm s^{-1}, at $r \sim 20$ km. The associated turnover times are thus $t_{\rm con} \simeq l_p/|v| \simeq 20$ ms, in good agreement with the estimate made above.

To isolate this effect from that due to viscosity (which generates the meridional circulations mentioned previously), we have performed a simulation in which $\alpha = 0$ (run aIM in Table 1). This calculation shows essentially no accretion onto the black hole except for a small amount of gas transferred at early times (because the initial condition is not in strict equilibrium). The result concerning the profile of Y_e as a function of radius is as we have described above, i.e., increasing neutronization as r decreases, until the opaque region is reached, followed by an increase in Y_e as the black hole boundary is approached. The revealing difference lies in the time evolution of this profile. As mentioned above, convection generates motions that tend to eliminate the composition gradient that drives it. In the presence of viscosity, matter is continuously transported radially, and the gradient is not erased entirely. Height-integrated profiles of $Y_e(r)$ at 50 and 200 ms show a similar behavior at small radii. When viscosity is removed, the initial composition gradient is gradually softened until it disappears in the innermost regions (see Fig. 7). The disk then has a nearly constant electron fraction along the equator for $r < r_*$, with a sharp transition region leading to an increase with radius in the transparent regime. This may resemble the convection-dominated accretion solution found analytically by Quataert & Gruzinov (2000) and numerically by several groups (Stone et al. 1999; Narayan et al. 2000), where convection transports angular momentum inward, energy outward, and gives a radial profile in density $\propto r^{-1/2}$. We find a different power law, with $\rho \propto r^{-1}$. There are several factors that may account for this difference: the disk versus spherical geometry, the initial condition with a large amount of internal energy, and the limited but present cooling rate on the boundaries of the flow.

3.3. *Neutrino Diffusion Effects*

Since the neutrinos are diffusing out of the fluid (the mean free path is small compared to the size of the system in the optically thick regime), one would expect a corresponding viscosity through $\zeta_\nu^{\rm vis}$ (see, e.g., Burrows et al. 1981). This needs to be compared to the corresponding viscosity generated by the assumed α prescription for consistency. We may assume $\zeta_\nu^{\rm vis} = \frac{1}{3} U_\nu l_\nu / c$, where $U_\nu \approx aT^4$ is the energy density associated with neutrinos and l_ν is their mean free path (see § 2.4). Thus,

$$\zeta_\nu^{\rm vis} \approx 2 \times 10^{20} \text{ g cm}^{-1} \text{ s}^{-1}, \tag{26}$$

for conditions near the equatorial plane, $z = 0$. This value will increase in the outer regions, since the mean free path becomes larger as the density drops. At the neutrino surface, where $\tau_\nu \approx 1$, the mean free path is $l_\nu \approx 10^7$ cm, and so an averaged value of the viscosity over the entire neutrino-opaque region will result in an increase of about 1 order of magnitude over the estimate given in equation (26) (note, however, that strictly speaking the diffusion approximation is no longer valid in the outer regions, so this must be interpreted with care). For the α prescription, $\zeta_\alpha = \rho \alpha c_s^2/\Omega$. The rotation curve is not too far from Keplerian, and scaling this expression to typical values, we find

$$\zeta_\alpha = 1.3 \times 10^{22} c_{s,9}^2 \alpha_{-2} r_7^{3/2} M_4^{-1/2} \rho_{10} \text{ g cm}^{-1} \text{ s}^{-1}. \tag{27}$$

The effects on angular momentum transport are thus a full 2 orders of magnitude below those arising from our viscosity prescription (for $\alpha = 10^{-2}$). To put it another way, a lower limit for the viscosity under these conditions (and in the optically thick portion of the disk) would be $\alpha \simeq 10^{-4}$. An alternative analysis would be to consider the corresponding timescales induced by this viscosity. Since $t_{\rm vis} \propto R(\rho/\zeta)^2$, smaller viscosities imply longer timescales, as expected.

3.4. *Stability*

Aside from convection, several general criteria for stability can be analyzed in our case. Evidently, since we are performing dynamical calculations, any instability that arises will quickly lead to a change in structure. It is nevertheless instructive to consider the corresponding conditions within the disk. We first consider the Toomre criterion, comparing gravitational and internal energies, with

$$Q_{\rm T} = \frac{\omega_r c_s}{\pi G \Sigma}, \tag{28}$$

where ω_r is the local epicyclic frequency (essentially equal in this case to the angular frequency Ω), c_s is the local sound speed,

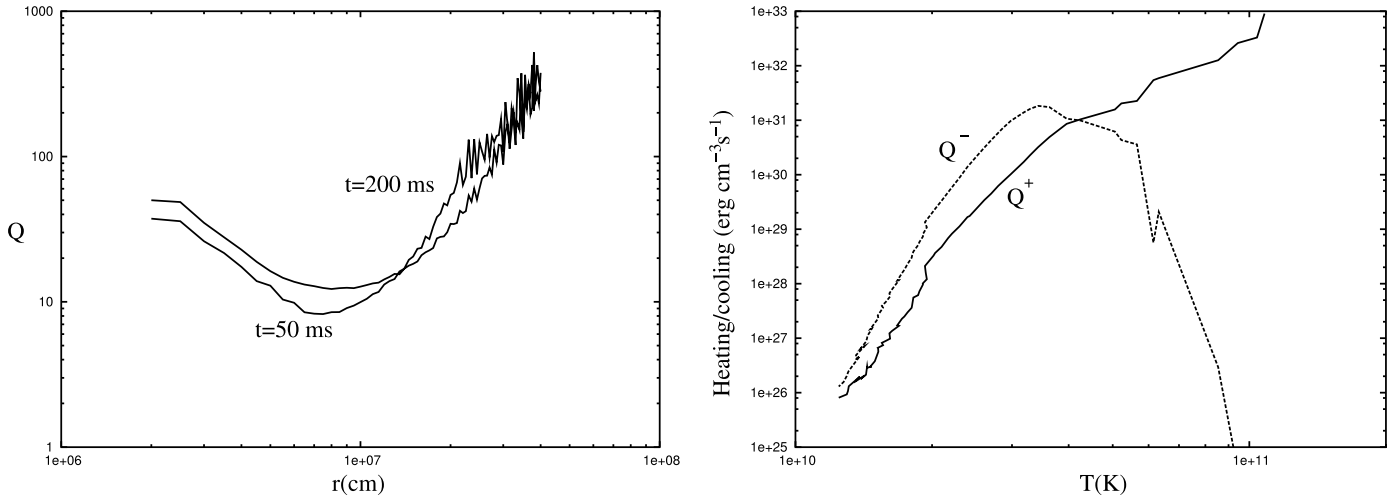

FIG. 8.—*Left*: Toomre parameter $Q_{\rm T}(r) = \omega_r c_s/\pi G\Sigma$ for run a2M at $t = 50$ and 200 ms. *Right*: Heating and cooling rates, Q^+ and Q^-, as a function of the central (equatorial) disk temperature, T_c, also for run a2M at $t = 50$ ms. See text for discussion.

and Σ is the surface density. We find $Q_{\rm T} > 1$ in all cases throughout the calculations and thus that the disks are stable in this respect [Fig. 8*a* shows a typical profile of $Q_{\rm T}(r)$].

Previous studies (Narayan et al. 2001; Kohri & Mineshige 2002) have shown that neutrino-cooled disks are thermally unstable if radiation pressure dominates in the flow and stable otherwise, although the effects of neutrino opacities were not considered. The criterion for stability can be written in this case as

$$\left(\frac{d\ln Q^+}{d\ln T}\right)_r \le \left(\frac{d\ln Q^-}{d\ln T}\right)_r, \tag{29}$$

where Q^+ and Q^- are the volume heating and cooling rates. Essentially, in order to be stable, the disk must be able to get rid of any excess internal energy generated by an increase in the heating rate. We show in Figure 8*b* typical values for Q^+ and Q^- as functions of the central (equatorial) temperature, for run a2M at $t = 50$ ms. In the optically thin region the disks are thermally stable because the pressure is dominated by the contribution from free nucleons and cooling is efficient. In the optically thick region the cooling is greatly suppressed and the criterion would indicate that the disk becomes thermally unstable. This is reasonable, since with optical depths $\tau_\nu \approx 10$–100, essentially no direct cooling takes place, and dissipation is not suppressed. This is why the disk is geometrically thick in the inner regions, as already described above (§ 3.1). The balance that gives a quasi–steady state structure is achieved mainly through the diffusion of neutrinos, since the diffusion timescale is shorter than the accretion timescale.

3.5. *Disk Evolution*

The evolution of the disk on long timescales is determined by the balance between two competing effects: On one hand, viscosity transports angular momentum outward, matter accretes, and the disk drains into the black hole on an accretion timescale $t_{\rm acc}$. The trend in this respect is toward lower densities and temperatures. On the other hand, cooling reduces pressure support and leads to vertical compression, increasing the density. The internal energy of the fluid is released on a cooling timescale, $t_{\rm cool}$. The presence of an optically thick region in the center of the disk limits the luminosity (dominated by electron and positron capture onto free nucleons) to approximately a few times 10^{53} ergs s^{-1}, and the initial internal energy is $E_{\rm int} \approx 10^{52}$ ergs, so $t_{\rm cool} \simeq 0.1$ s. If $t_{\rm acc} > t_{\rm cool}$, the disk will cool before its mass or internal energy reservoir is significantly affected by accretion onto the black hole. The maximum density (shown in Fig. 9 for runs a1M, a2M, and a3M) actually increases slightly due to vertical compression and subsequently drops once mass loss through accretion dominates (the $\simeq$10 ms delay at the start, during which it is approximately constant, is simply the sound crossing time across the optically thick region of the disk). The accretion rate onto the black hole $\dot{M}_{\rm BH}$, the accretion timescale $t_{\rm acc} = \dot{M}_{\rm BH}/M_{\rm disk}$, and the total neutrino luminosity L_ν are shown in Figures 10, 11, and 12. They all show the same qualitative behavior, remaining fairly constant (or changing slowly) for an accretion timescale and abruptly switching thereafter. The accretion timescales are approximately 0.5 and 5 s for $\alpha = 0.01$ and 0.001, respectively.

For high viscosity, $\alpha = 0.1$, the transport of angular momentum is vigorous, and the black hole quickly accretes a substantial amount of mass (0.16 $M_\odot$ within the first 100 ms). The accretion timescale is $t_{\rm acc} \simeq 50$ ms. The circulation pattern consists of large-scale eddies, with $H \simeq r$. In fact, there is essentially one large eddy on each side of the equatorial plane, with mass inflow along the surface of the disk and an equatorial outflow. Part of the

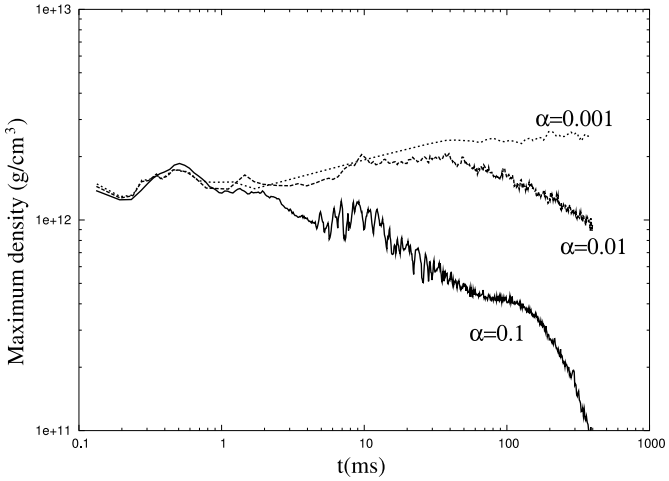

FIG. 9.—Maximum density, $\rho_{\rm max}$, in the accretion disk for runs a1M, a2M, and a3M.

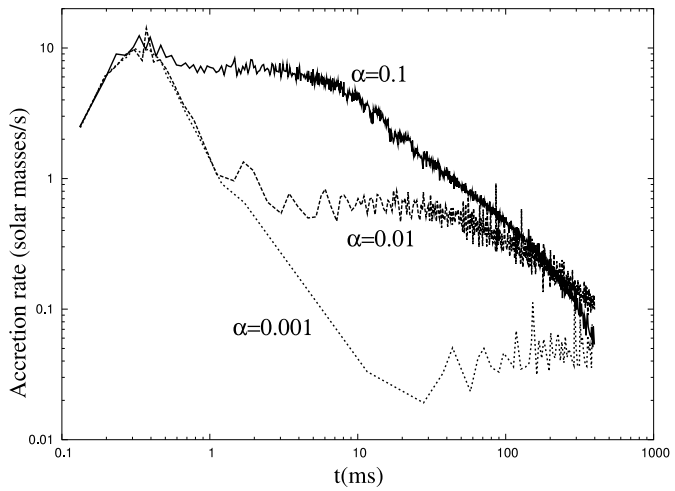

FIG. 10.—Net accretion rate (in $M_\odot$ s^{-1}) onto the black hole as a function of time for runs a1M, a2M, and a3M.

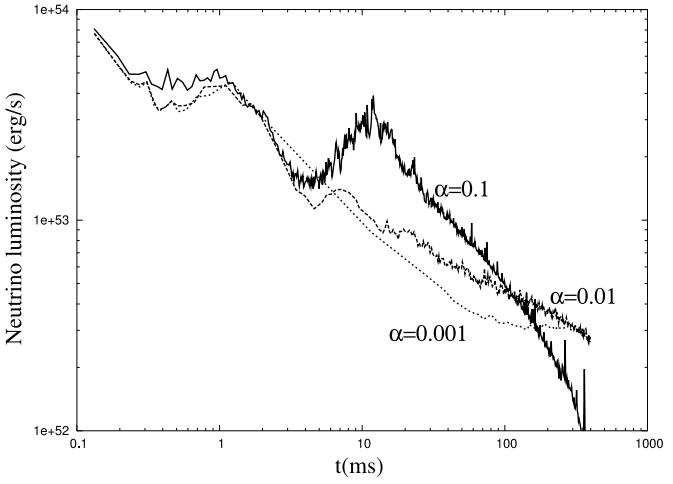

FIG. 12.—Neutrino luminosity L_ν, computed from eq. (22), for runs a1M, a2M, and a3M. Note the fairly flat curves and rise, for run a1M at early times, when the disk is optically thick and the transition to the optically thin regime at a later time. The curves for runs a2M and a3M exhibit a break approximately on the cooling timescale, $t_{\rm cool}$.

outflowing gas moves away from the equator and reverses direction close to the surface of the disk, contributing to the inflow. For an intermediate viscosity, $\alpha = 0.01$, the intensity of the circulations is smaller, but also the eddies are smaller, with several of them clearly occurring in the disk at once. The transport of angular momentum being less vigorous, the accretion rate is substantially smaller than in the previous case. Finally, for a yet lower viscosity, $\alpha = 0.001$, the trend continues, and the eddies become smaller still. In these last two cases, angular momentum transport is so low that very high densities are maintained in the central regions of the disk for a large number of dynamical times, contrary to what is seen in the high-viscosity case. A simple way to quantify how much of the mass flow is actually making it to the central black hole is to measure the fraction of mass at any given radius that is moving inward, $|\dot{M}_{\rm in}|/(|\dot{M}_{\rm in}| + |\dot{M}_{\rm out}|)$, where we have divided the mass flow rate into two height-integrated parts, one with $v_r < 0$ and another with $v_r > 0$. For example, for run a2M at $t = 100$ ms and $r = r_*$ it is approximately $\frac{1}{3}$. The ratio tends to unity only in the innermost regions of the disk and shows the true black hole mass accretion rate, plotted in Figure 10 for the same cases.

We now turn our attention to the neutrinos, which are the main source of cooling. The results in this case are markedly different from what we initially found (Lee & Ramirez-Ruiz 2002), simply because of the new equation of state, the more realistic cooling rates, and the approximate computation of opacities. They are in general agreement with the preliminary results we presented before (Lee et al. 2004), which used a less detailed equation of state than the one shown here.

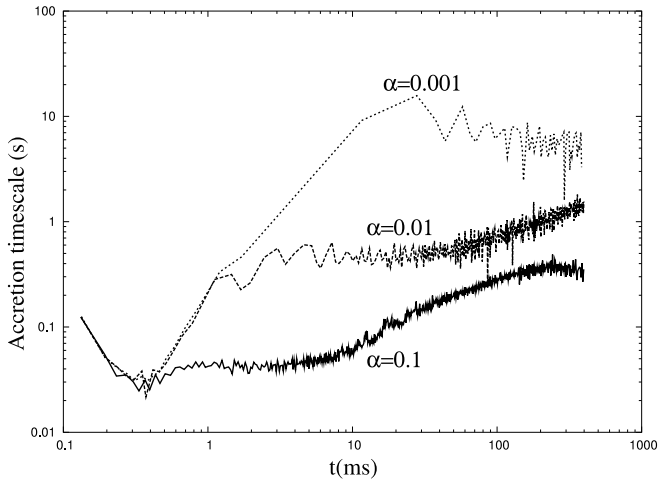

FIG. 11.—Accretion timescale, $M_d/\dot{M}_{\rm BH}$, in seconds and as a function of time for runs a1M, a2M, and a3M.

The optically thick region is present in every disk at the start of the calculation. As already mentioned, this has two important effects: enhancing the pressure and suppressing the neutrino emission. This reflects on the total luminosity, since the suppression occurs precisely in the hottest regions, where most of the energy would otherwise be released. The most important qualitative difference between the runs presented here is that for a high viscosity ($\alpha = 0.1$, runs a1M and a1m) the disk is drained of mass so fast that it has no chance to cool ($t_{\rm acc} < t_{\rm cool}$) and release most of its internal energy. It is in fact advected into the black hole. Moreover, the optically thick region disappears entirely from the disk (see Fig. 5) by $t = 40$ ms. The emission is then no longer suppressed (see the contours of $\dot{q}$ in the same figure), and the disk radiates at the maximum possible cooling rate. The thermal energy content of the disk is so large that, as it thins, the luminosity actually increases briefly around $t = 10$ ms before dropping again. The drop at late times follows an approximate power law, with $L_\nu \propto t^{-1}$. In this interval the energy release comes from a combination of residual internal energy and viscous dissipation within the disk. For lower values of the viscosity, $\alpha \leq 0.01$, the central regions of the disk remain optically thick throughout the calculations. Note that reducing the disk mass by a factor of 5 (as was done for runs a1m, a2m, and a3m) does not affect these overall conclusions. The fluid is simply compressed into a smaller volume, and thus the densities and temperatures that are reached are similar to those for the high-mass runs. For run a3M the neutrino luminosity is practically constant at $2. \times 10^{52}$ ergs s^{-1} for $t \geq 100$ ms. Table 2 summarizes the typical disk mass, energy density, accretion rate, luminosity, and duration and energetics of neutrino emission for all runs.

4. SUMMARY, CONCLUSIONS, AND ASTROPHYSICAL IMPLICATIONS

4.1. *Summary*

We have performed two-dimensional hydrodynamical simulations of accretion disks in the regime of hypercritical accretion,

TABLE 2
ACCRETION DISK PARAMETERS DURING THE DYNAMICAL EVOLUTION

Run	$\dot{M}$ ($M_\odot$ s^{-1})	ρc_s^2 (ergs cm^{-3})	L_ν (ergs s^{-1})	E_ν[a] (ergs)	E_ν[b] (MeV)	$T_{\nu,1/2}$[c] (ms)	$M_{\rm disk}$[a] ($M_\odot$)
aIM	0	6×10^{30}	2×10^{52}	1.5×10^{52}	8	>140[d]	0.308
a1M	7	2×10^{31}	2×10^{53}	2×10^{52}	8	60	0.098
a2M	0.7	2×10^{31}	6×10^{52}	2×10^{52}	8	150	0.2
a3M	0.05	1.6×10^{31}	$2. \times 10^{52}$	1.55×10^{52}	8	>140[d]	0.287
a1m	0.7	4×10^{30}	2×10^{52}	5.4×10^{51}	8	25	0.022
a2m	0.05	3×10^{30}	1×10^{52}	5.5×10^{51}	8	75	0.045
a3m	0.005	3×10^{30}	1.5×10^{52}	7×10^{51}	8	>160[d]	0.059

[a] Values are given at $t = 0.4$ s.
[b] The typical neutrino energy is given at the radius where $\tau_\nu = 1$.
[c] This is the duration of the neutrino emission, measured as the time needed for the disk to release one-half of E_ν.
[d] This is a lower limit, since for $\alpha = 0.001$ the disk is still in a quasi–steady state at $t = 0.2$ s and has not yet drained into the black hole.

where neutrino emission is the main cooling agent. The disks are assumed to be present around a stellar-mass black hole and are evolved for a few hundred dynamical timescales. We have paid particular attention to the relevant microphysical processes under the conditions at hand and used a detailed equation of state that includes an ideal gas of α-particles and free baryons in nuclear statistical equilibrium and a relativistic Fermi gas of arbitrary degeneracy. The composition of the fluid is determined by weak interactions. The density and temperature are such that the inner regions of the disk become opaque to neutrinos, and this is taken into account in a simple approximation.

4.2. *Conclusions*

Our main conclusions can be summarized as follows:

1. Once the fluid becomes photodisintegrated into free nucleons, neutronization becomes important and lowers the electron fraction substantially below $\frac{1}{2}$, with the electron fraction Y_e reaching $\approx$0.05 at its minimum. This value, however, does not occur in the immediate vicinity of the black hole, but rather at the transition radius where the fluid becomes optically thick to its own neutrino emission, $r_* \approx 10^7$ cm. At smaller radii, the electron fraction rises again, reaching $\approx$0.1 close to the horizon.

2. Neutrino trapping produces a change in composition and an inversion in the electron fraction. The associated negative gradient in $Y_e(r)$ induces convective motions in the optically thick region of the disk. This is analogous to what presumably occurs following core collapse, in a proto–neutron star and its surrounding envelope. Due to the radial flows induced by viscosity, convection is unable to suppress this composition gradient. It would appear, however, that the entropy per baryon in the optically thick region is very close to being constant, with $s/k \approx 6$.

3. The spatial structure of the disk is characterized by the transition radius r_* where the material becomes optically thick. For $r > r_*$ the disk cools efficiently, whereas for $r < r_*$ the emission is suppressed and the fluid is unable to cool directly (although it does so on a neutrino diffusion timescale). This leads to larger pressures and a more moderate rise in density.

4. The temporal evolution of the disk is determined by the balance between accretion and neutrino emission. For low viscosities ($\alpha \leq 0.01$), the disk is able to cool in a quasi–steady state and radiate its internal energy reservoir. This lasts for approximately 0.1–0.4 s, with $L_\nu \approx 10^{53}$ ergs s^{-1}. Thereafter the typical luminosity and density quickly decay. For large viscosities ($\alpha \simeq 0.1$) the disk is drained of mass on an accretion timescale that is shorter than the cooling timescale, and the internal energy of the disk is essentially advected into the black hole. An interesting result in this case is that as the disk becomes transparent before being engulfed by the hole, it undergoes a rebrightening, as some of the stored energy escapes.

5. The total energy output in neutrinos is $E_\nu \approx 10^{52}$ ergs, over a timescale of $\approx$400 ms. The typical accretion rates are $\approx$0.1 $M_\odot$ s^{-1}, and neutrino energies are $\approx$8 MeV at r_*. Energy densities in the inner regions of the disk are $\approx 10^{31}$ ergs cm^{-3}.

4.3. *Discussion*

There are two main ingredients in the results presented here that contrast with those available previously in the literature concerning the steady state structure of neutrino-cooled accretion disks. The first is the ability to dynamically model the evolution of the system for hundreds of dynamical timescales, taking the previous history of the fluid into consideration through the choice of initial conditions. This allows us to consider the energetics on more relevant timescales (cooling, viscous) than the dynamical one accessible in three-dimensional studies. The second is the realization that the structure of the disks is affected qualitatively by the presence of an optically thick region at high densities. In this sense the situation is similar to that encountered following massive core collapse, where convection occurs (recent work assessing the relative importance of the MRI, neutrino, and convection-driven viscosity in rotating collapsing cores has been reported by Akiyama et al. 2003; Thompson et al. 2005; we comment further on this issue in § 4.3.2).

Clearly there is room for improvement in the results presented here. To begin with, our expressions for the effect of a finite optical depth on cooling and pressure are too simple and attempt only to capture the essential physical behavior of the system. There is an important region of the disk where the optical depth is not large enough to consider the diffusion approximation and where more detailed transport effects ought to be considered. We have not separated the neutrino variables into three species, which would be more rigorous (e.g., Yokosawa et al. [2004] have noted that in such flows, the electron neutrinos ν_e might be preferentially absorbed with respect to electron antineutrinos $\overline{\nu}_e$, thus affecting the neutrino annihilation luminosity above the surface of the disk in an important way). We have only considered the effects of coherent scattering off nucleons and α-particles for opacity purposes. This specifically ignores absorptive scattering, which would (1) lead to a modification of the neutrino emergent spectrum and (2) produce heating of the fluid. The latter may be particularly important concerning the driving of powerful

winds off the surface of the disk and needs to be addressed more carefully in the context of GRBs. As in previous work, we have chosen to maintain the Newtonian expression for the potential well of the central black hole for ease of comparison to previous results (this will be addressed in future work).

4.3.1. *Gamma-Ray Bursts*

The sudden release of gravitational binding energy of a neutron star is easily sufficient to power a GRB. The minimum energy requirement is $10^{51}(\Delta\Omega/4\pi)$ ergs if the burst is beamed into a solid angle $\Delta\Omega$. As discussed in § 1, a familiar possibility, especially for bursts belonging to the short-duration category, is the merger of a neutron star and a black hole, or double neutron star binary by emission of gravity waves, which, as illustrated here, is likely to generate a black hole surrounded by a lower mass accretion disk. How is the available rotational and gravitational energy converted into an outflowing relativistic plasma? A straightforward way is that some of the energy released as thermal neutrinos is reconverted, via collisions outside the disk, into electron-positron pairs or photons. The neutrino luminosity emitted when disk material accretes via viscous (or magnetic) torques on a timescale $\Delta t \sim 1$ s is roughly

$$L_\nu \sim 2\times 10^{52}\left(\frac{M_{\rm disk}}{0.1\ M_\odot}\right)\left(\frac{\Delta t}{1\ {\rm s}}\right)^{-1}\ {\rm ergs\ s^{-1}} \qquad (30)$$

for a canonical radiation efficiency of 0.1. During this time, the rate of mass supply to the central black hole is of course much greater than the Eddington rate. Although the gas photon opacities are large, the disk becomes sufficiently dense and hot to cool via neutrino emission. There is in principle no difficulty in dissipating the disk internal energy, but the problem is in allowing these neutrinos to escape from the inflowing gas. At sufficiently low accretion rates, $\alpha \lesssim 0.01$, we find that the energy released by viscous dissipation is almost completely radiated away on a timescale given by $t_{\rm cool} \approx E_{\rm int}/L_\nu \sim 0.1$ s. In contrast, for a higher mass supply, $\alpha \gtrsim 0.1$, energy advection remains important until the entire disk becomes optically thin. The restriction on the cooling rate imposed by high optical depths is key because it allows the energy loss to be spread over an extended period of time during which the neutrino luminosity stays roughly constant. This gives a characteristic timescale for energy extraction and may be essential for determining the duration of neutrino-driven short GRBs (Lee et al. 2004).

Neutrinos could give rise to a relativistic pair-dominated wind if they converted into pairs in a region of low baryon density (e.g., along the rotation axis, away from the equatorial plane of the disk). The $\nu\bar{\nu} \rightarrow e^+e^-$ process can tap the thermal energy of the torus produced by viscous dissipation. For this mechanism to be efficient, the neutrinos must escape before being advected into the hole; on the other hand, the efficiency of conversion into pairs (which scales with the square of the neutrino density) is low if the neutrino production is too gradual. Typical estimates suggest a lower bound[6] of $L_{\nu\bar{\nu}} \sim 10^{-3}L_\nu$ (e.g., Rosswog & Ramirez-Ruiz 2003). If the pair-dominated plasma were collimated into a solid angle $\Delta\Omega$, then of course the apparent isotropized energy would be larger by a factor $(4\pi/\Delta\Omega)$, but unless $\Delta\Omega$ is $\leq 10^{-2}$, this may fail to satisfy the apparent isotropized energy of 10^{52} ergs implied by a redshift $z = 1$ for short GRBs.

One attractive mechanism for extracting energy that could circumvent the above efficiency problem is a relativistic magnetohydrodynamic (MHD) wind (Usov 1992; Thompson 1994). Such a wind carries both bulk kinetic energy and ordered Poynting flux, and it is possible that gamma-ray production occurs mainly at large distances from the source (Duncan & Thompson 1992; Usov 1994; Thompson 1994). A rapidly rotating neutron star (or disk) releases energy via magnetic torques at the rate $L_{\rm mag} \sim 10^{49}B_{15}^2P_{-3}^{-4}R_6^6$ ergs s^{-1}, where $P = 10^{-3}P_{-3}$ s is the spin period and $B = 10^{15}B_{15}$ G is the strength of the poloidal field at a radius $R = 10^6R_6$ cm. The last stable orbit for a Schwarzschild hole lies at a coordinate distance $R = 6GM/c^2 = 9(M/M_\odot)$ km, to be compared with $R = GM/c^2 = 3/2(M/M_\odot)$ km for an extremal Kerr hole. Thus, the massive neutron disk surrounding a Schwarzschild black hole of approximately 2 $M_\odot$ should emit a spin-down luminosity comparable to that emitted by a millisecond neutron star. A similar MHD outflow would result if angular momentum were extracted from a central Kerr hole via electromagnetic torques (Blandford & Znajek 1977). The field required to produce $L_{\rm mag} \geq 10^{51}$ ergs s^{-1} is colossal and may be provided by a helical dynamo operating in hot, convective nuclear matter with a millisecond period (Duncan & Thompson 1992). A dipole field of the order of 10^{15} G appears weak compared to the strongest field that can in principle be generated by differential rotation [$\sim 10^{17}(P/1\ {\rm ms})^{-1}$ G] or by convection ($\sim 10^{16}$ G), although how this may come about in detail is not resolved. We examine in more detail the possible generation of strong magnetic fields in § 4.3.2.

Computer simulations of compact object mergers and black hole formation can address the fate of the bulk of the matter, but there are some key questions that they cannot yet tackle. In particular, high resolution of the outer layers is required because even a tiny mass fraction of baryons loading down the outflow severely limits the attainable Lorentz factor: for instance, a Poynting flux of 10^{53} ergs could not accelerate an outflow to $\Gamma \gtrsim 100$ if it had to drag more than $\sim 10^{-4}\ M_\odot$ of baryons with it. One further effect renders the computational task of simulating jet formation even more challenging. This stems from the likelihood that the high neutrino fluxes ablate baryonic material from the surface of the disk at a rate (Qian & Woosley 1996)

$$\dot{M}_\eta \sim 5\times 10^{-4}\left(\frac{L_\nu}{10^{52}\ {\rm ergs\ s^{-1}}}\right)^{5/3} M_\odot\ {\rm s^{-1}}. \qquad (31)$$

A rest-mass flux $\dot{M}_\eta$ limits the bulk Lorentz factor of the wind to

$$\Gamma_\eta = \frac{L_{\rm mag}}{\dot{M}_\eta c^2} = 10\left(\frac{L_{\rm mag}}{10^{52}\ {\rm ergs\ s^{-1}}}\right)\left(\frac{\dot{M}_\eta}{5\times 10^{-4}\ M_\odot\ {\rm s^{-1}}}\right)^{-1}. \qquad (32)$$

If one assumes that the external poloidal field strength is limited by the vigor of the convective motions, then the spin-down luminosity scales with neutrino flux as $L_{\rm mag} \propto B^2 \propto v_{\rm con}^2 \propto L_\nu^{2/3}$, where $v_{\rm con}$ is the convective velocity. The ablation rate given in equation (31) then indicates that the limiting bulk Lorentz factor Γ_η of the wind decreases as L_ν^{-1}. Thus, the burst luminosity emitted by a magnetized neutrino-cooled disk may be self-limiting. The mass loss would, however, be suppressed if the relativistic wind were collimated into a jet. This suggests that centrifugally driven mass loss will be heaviest in the outer

[6] This estimate, however, assumes that the entire surface area emits close to a single-temperature blackbody. It should be noted that if the dissipation takes place in a corona-like environment, the efficiency may be significantly larger (Ramirez-Ruiz & Socrates 2005).

parts of the disk and that a detectable burst may be emitted only within a certain solid angle centered on the rotation axis (see, e.g., Rosswog & Ramirez-Ruiz 2003).

4.3.2. *Generation of Strong Magnetic Fields*

There is also the question of magnetic fields, which we have not included but should obviously be considered. The field in a standard disk is probably responsible for viscous stresses and dissipation, through the MRI. In this respect the current scenario should exhibit these characteristics. The MRI operates on an orbital timescale, and so the field would grow in a few tens of milliseconds. It may also be amplified by the convective motions described in § 3.2. The saturation value for the field can be naively estimated as that at which its energy density is in equipartition with the gas, $B^2/8\pi \approx \rho c_s^2$, or when the Alfvén speed, $v_{\rm A} = B/(4\pi\rho)^{1/2}$, is comparable to the azimuthal velocity, v_ϕ. This gives $B \approx 10^{16}$ G. It is not clear at all, however, that the field amplitude will reach such high levels because the magnetic Reynolds number is far beyond its critical value (where diffusion balances dynamo-driven growth), and amplification can lead to field expulsion from the convective region, thereby destroying the dynamo (Rädler et al. 2002). Precious little is known about the growth of magnetic fields at such overcritical levels (Reinhardt & Geppert 2005), and a definitive answer will require the self-consistent inclusion of full MHD into the problem at hand (but with a level of resolution that may be well above present computational capabilities). It is not clear either that the magnetic shearing instability can generate a mean poloidal field as strong as $B \approx 10^{16}$ G, since to first order it does not amplify the total magnetic flux. The nonlinear evolution of the instability depends sensitively on details of magnetic reconnection, and it has indeed been suggested that this can smooth reversals in the field on very small scales, pushing the dominant growing mode to much larger scales (Goodman & Xu 1994).

It is certainly possible, as shown here, that compact binary mergers do form a neutron disk that is hot enough to be optically thick to neutrinos, and convective instability is a direct consequence of the hot nuclear equation of state. A neutron disk is likely to be convective if the accretion luminosity exceeds 10^{50}–10^{51} ergs s^{-1}. Note that even if the accretion luminosity is lower, a hot, massive disk (such as those forming in collapsars; Woosley 1993) would undergo a brief period of convection as a result of secular cooling (notice that convection is driven by secular neutrino cooling, whereas the MRI is powered by a release of shear kinetic energy). If the dense matter rotates roughly at the local Keplerian angular velocity, $\Omega \simeq (GM_{\rm BH}/r^3)^{1/2}$, then $L_{\rm mag}$ is approximately independent of radius, and the required poloidal field for a given luminosity is $B_{15} \approx L_{\rm mag,50}^{1/2}(M_{\rm BH}/M_\odot)^{-1}$. If a period of convection is a necessary step in the formation of a strong, large-scale poloidal field, an acceptable model thus requires that the surrounding torus should not completely drain into the hole on too short of a timescale. Whether a torus of given mass survives clearly depends on its thickness and stratification, which in turn depends on internal viscous dissipation and neutrino cooling.

A large amount of differential rotation (as may occur in newborn neutron stars or those in X-ray binaries and is definitely the case in toroidal structures supported mainly by centrifugal forces), combined with short periods, may produce substantial magnetic field amplification (Kluźniak & Ruderman 1998; Spruit 1999). The energy transferred to the magnetic field is released in episodic outbursts when the buoyancy force allows the field to rise to the surface of the star or disk. The amplification of a magnetic field to such strong values would clearly have important consequences on the evolution and time variability of the disk and its energy output. It would probably lead to strong flaring and reconnection events accompanied by the release of large amounts of energy, if the growth time for field amplification, t_B, is shorter than the accretion timescale, $t_{\rm acc}$ (otherwise the disk would drain of matter before the field had the chance to reach large values; in this case, the survival of a massive, rapidly rotating neutron star as the end point of binary neutron star merger might be preferred over the prompt formation of a BH). An effective helical dynamo of the α-Ω type should be favored by a low effective viscosity, α, because, as stated in § 3.2, the overturn time[7] is $t_{\rm con} \approx 20$ ms (this applies only if the disk is not fed with matter externally for a time longer than $t_{\rm acc}$, otherwise convection would also be able to amplify the magnetic field).

4.3.3. *Nucleosynthesis*

Core-collapse SNe and compact object mergers are natural astrophysical sites for the production of heavy elements (Lattimer & Schramm 1974; Meyer & Brown 1997; Freiburghaus et al. 1999; Rosswog et al. 1999; Lee 2001). In particular, nucleosynthesis in neutrino-driven winds is an issue that may be relevant for iron-group elements, as well as for heavier nuclei through the *r*-process (Woosley & Hoffman 1992). Initial investigations into this matter (Qian & Woosley 1996) determined that the entropy in the outflow arising from a newborn neutron star was probably too low to give rise to the *r*-process efficiently. More recently, this problem has been addressed again in the specific case of collapsar or postmerger accretion disks, based on the results of analytical calculations of neutrino-cooled disks in one dimension (Pruet et al. 2004). If the wind consists of a uniform outflow driven from the surface of the disk, the entropy is too low, and essentially only iron-group elements are synthesized, in agreement with the earlier results. However, their results also indicate that in a bubble-type outflow (against a background steady wind), where episodic expulsion of material from the inner regions takes place, material may be ejected from the disk and preserve its low electron fraction, thus allowing the *r*-process to occur. The convective motions reported here, occurring in the optically thick portion of the disk, would represent one way such cells could be transported to the disk surface if they can move fast enough to preserve the neutron excess. Since the existence of a convection region is dependent on the densities reached in the inner disk (so that it becomes opaque), the synthesized nuclei (iron group vs. heavier, *r*-process elements) could be a reflection of its absence/presence.

We have benefited from many useful discussions and correspondence with U. Geppert, N. Itoh, K. Kohri, P. Kumar, A. MacFadyen, P. Mészáros, M. Prakash, M. Rees, T. Thompson, S. Woosley, and A. Socrates. Financial support for this work was provided in part by CONACyT 36632E (W. H. L., D. P.) and by NASA through a Chandra Postdoctoral Fellowship award PF3-40028 (E. R.-R.). Part of this work was done during visits to the Institute for Advanced Study (W. H. L.) and Instituto de Astronomía, UNAM (E. R.-R.), whose hospitality is gratefully acknowledged. We thank the anonymous referee for helpful comments and suggestions on the initial manuscript.

[7] Recall that the resulting convective motions in a proto–neutron star are extremely vigorous, with an overturn time of $\sim$1 ms.

REFERENCES

Abramowicz, M. A. 2004, in Growing Black Holes: Accretion in a Cosmological Context, ed. A. Merloni, S. Nayakshin, & R. Sunyaev (Berlin: Springer), 257
Abramowicz, M. A., Chen, X., Kato, Y., Lasota, J. P., & Regev, O. 1995, ApJ, 438, L37
Akiyama, S., Wheeler, J. C., Meier, D. L., & Lichtenstadt, I. 2003, ApJ, 584, 954
Arlt, R., & Urpin, V. 2004, A&A, 426, 755
Balbus, S. A., & Hawley, J. F. 1991, ApJ, 376, 214
Beloborodov, A. M. 2003, ApJ, 588, 931
Berger, E., Kulkarni, S., & Frail, D. A. 2003, ApJ, 590, 379
Blandford, R. D., & Znajek, R. L. 1977, MNRAS, 179, 433
Blinnikov, S. I., Dunina-Barkovskaya, N. V., & Nadyozhin, D. K. 1996, ApJS, 106, 171
Burrows, A., & Lattimer, J. M. 1986, ApJ, 307, 178
Burrows, A., Mazurek, T. J., & Lattimer, J. M. 1981, ApJ, 251, 325
Chevalier, R. A. 1989, ApJ, 346, 847
DiMatteo, T., Perna, R., & Narayan, R. 2002, ApJ, 579, 706
Duncan, R. C., & Thompson, C. 1992, ApJ, 392, L9
Eichler, D., Livio, M., Piran, T., & Schramm, D. N. 1989, Nature, 340, 126
Epstein, R. I. 1979, MNRAS, 188, 305
Frail, D. A., et al. 2001, ApJ, 562, L55
Freiburghaus, C., Rembges, J.-F., Rauscher, T., Kolbe, E., & Thielemann, F.-K. 1999, ApJ, 516, 381
Goodman, J., & Xu, G. 1994, ApJ, 432, 213
Hannestad, S., & Raffelt, G. 1998, ApJ, 507, 339
Hawley, J. F., & Balbus, S. A. 1991, ApJ, 376, 223
Hjorth, J., et al. 2003, Nature, 423, 847
Houck, J. C., & Chevalier, R. A. 1991, ApJ, 376, 234
Hulse, R. A., & Taylor, J. H. 1975, ApJ, 195, L51
Ichimaru, S. 1977, ApJ, 214, 840
Itoh, N., Hayashi, H., Nishikawa, A., & Kohyama, Y. 1996, ApJS, 102, 411
Janka, H.-Th., & Müller, E. 1996, A&A, 306, 167
King, A., & Dehnen, W. 2005, MNRAS, 357, 275
Kita, D. B. 1995, Ph.D. thesis, Univ. Wisconsin-Madison
Kluźniak, W., & Kita, D. 2000, preprint (astro-ph/0006266)
Kluźniak, W., & Lee, W. H. 1998, ApJ, 494, L53
Kluźniak, W., & Ruderman, M. 1998, ApJ, 505, L113
Kohri, K., & Mineshige, S. 2002, ApJ, 577, 311
Kouveliotou, C., Meegan, C. A., Fishman, G. J., Bhat, N. P., Briggs, M. S., Koshut, T. M., Paciesas, W. S., & Pendleton, G. N. 1993, ApJ, 413, L101
Kulkarni, S., et al. 1998, Nature, 395, 663
Langanke, K., & Martínez-Pinedo, G. 2001, At. Data Nucl. Data Tables, 79, 1
Lattimer, J. M., & Mazurek, T. J. 1981, ApJ, 246, 955
Lattimer, J. M., & Schramm, D. N. 1974, ApJ, 192, L145
———. 1976, ApJ, 210, 549
Lazzati, D., Ramirez-Ruiz, E., & Ghisellini, G. 2001, A&A, 379, L39
Lee, W. H. 2001, MNRAS, 328, 583
Lee, W. H., & Ramirez-Ruiz, E. 2002, ApJ, 577, 893
Lee, W. H., Ramirez-Ruiz, E., & Page, D. 2004, ApJ, 608, L5
MacFadyen, A. I., & Woosley, S. E. 1999, ApJ, 524, 262
Mészáros, P. 2002, ARA&A, 40, 137
Meyer, B. S., & Brown, J. S. 1997, ApJS, 112, 199
Monaghan, J. J. 1992, ARA&A, 30, 543
Narayan, R., Igumenshchev, I. V., & Abramowicz, M. A. 2000, ApJ, 539, 798
Narayan, R., Paczyński, B., & Piran, T. 1992, ApJ, 395, L83
Narayan, R., Piran, T., & Kumar, P. 2001, ApJ, 557, 949
Narayan, R., & Yi, I. 1994, ApJ, 428, L13
———. 1995, ApJ, 452, 710
Paczyński, B. 1986, ApJ, 308, L43
———. 1991, Acta Astron., 41, 257
Panaitescu, A., & Kumar, P. 2001, ApJ, 560, L49
Piran, T. 2004, Rev. Mod. Phys., 76, 1143
Popham, R., Woosley, S. E., & Fryer, C. 1999, ApJ, 518, 356
Pruet, J., Thompson, T. A., & Hoffman, R. D. 2004, ApJ, 606, 1006
Pruet, J., Woosley, S. E., & Hoffman, R. D. 2003, ApJ, 586, 1254
Qian, Y.-Z., & Woosley, S. E. 1996, ApJ, 471, 331
Quataert, E., & Gruzinov, A. 2000, ApJ, 545, 842
Rädler, K.-H., Reinhardt, M., Apstein, E., & Fuchs, H. 2002, Magnetohydrodynamics, 38, 41
Ramirez-Ruiz, E., & Socrates, A. 2005, ApJ, submitted (astro-ph/0504257)
Rappaport, S. A., Podsiadlowski, P., & Pfahl, E. 2005, MNRAS, 356, 401
Regev, O., & Gitelman, L. 2002, A&A, 396, 623
Reinhardt, M., & Geppert, U. 2005, A&A, 435, 201
Rosswog, S., Liebendorfer, M., Thielemann, F.-K., Davies, M. B., Benz, W., & Piran, T. 1999, A&A, 341, 499
Rosswog, S., & Ramirez-Ruiz, E. 2002, MNRAS, 336, L7
———. 2003, MNRAS, 343, L36
Rosswog, S., Ramirez-Ruiz, E., & Davies, M. B. 2003, MNRAS, 345, 1077
Rosswog, S., Speith, R., & Wynn, G. A. 2004, MNRAS, 351, 1121
Ruffert, M., & Janka, H.-T. 1999, A&A, 344, 573
Ruffert, M., Janka, H.-T., & Schäfer, G. 1996, A&A, 311, 532
Salpeter, E. E. 1964, ApJ, 140, 796
Setiawan, S., Ruffert, M., & Janka, H.-Th. 2004, MNRAS, 352, 753
Shakura, N. I., & Sunyaev, R. A. 1973, A&A, 24, 337
Shapiro, S. L., Lightman, A. P., & Eardley, D. M. 1976, ApJ, 204, 187
Shapiro, S. L., & Teukolsky, S. A. 1983, Black Holes, White Dwarfs, and Neutron Stars (New York: Wiley)
Socrates, A., Blaes, O., Hungerford, A., & Fryer, C. L. 2004, ApJ, submitted (astro-ph/0412144)
Spiegel, E. A. 1972, ARA&A, 10, 261
Spruit, H. C. 1999, A&A, 341, L1
Stanek, K., et al. 2003, ApJ, 591, L17
Stone, J. M., Pringle, J. E., & Begelman, M. C. 1999, MNRAS, 310, 1002
Tassoul, J. L. 1978, Theory of Rotating Stars (Princeton: Princeton Univ. Press)
Thompson, C. 1994, MNRAS, 270, 480
Thompson, C., & Duncan, R. C. 1993, ApJ, 408, 194
Thompson, T. A., Quataert, E., & Burrows, A. 2005, ApJ, 620, 861
Tubbs, D. L., & Schramm, D. N. 1975, ApJ, 201, 467
Urpin, V. 1984, Soviet Astron. Lett., 28, 50 (English transl. in AZh, 61, 84)
Usov, V. V. 1992, Nature, 357, 472
———. 1994, MNRAS, 267, 1035
van Paradijs, J., Kouveliotou, C., & Wijers, R. A. M. J. 2000, ARA&A, 38, 379
Woosley, S. E. 1993, ApJ, 405, 273
Woosley, S. E., & Hoffman, R. D. 1992, ApJ, 395, 202
Yokosawa, M., Uematsu, S., & Abe, J. 2004, preprint (astro-ph/0412558)
Zel'dovich, Ya. B. 1964, Soviet Phys. Dokl., 9, 195 (English transl. in Dokl. Akad. Nauk SSSR, 155, 67)
Zhang, B., & Mészáros, P. 2004, Int. J. Mod. Phys. A, 19, 2385